

NIRVAR: Network Informed Restricted Vector Autoregression

Brendan Martin¹, Francesco Sanna Passino¹, Mihai Cucuringu^{2,3,4}, and Alessandra Luati^{1,5}

¹Department of Mathematics, Imperial College London, United Kingdom

²Department of Statistics, University of Oxford, United Kingdom

⁴Oxford-Man Institute of Quantitative Finance, University of Oxford, United Kingdom

⁴The Alan Turing Institute, London, United Kingdom

⁵Department of Statistical Sciences, University of Bologna, Italy

Abstract

High-dimensional panels of time series arise in many scientific disciplines such as neuroscience, finance, and macroeconomics. Often, co-movements within groups of the panel components occur. Extracting these groupings from the data provides a course-grained description of the complex system in question and can inform subsequent prediction tasks. We develop a novel methodology to model such a panel as a restricted vector autoregressive process, where the coefficient matrix is the weighted adjacency matrix of a stochastic block model. This network time series model, which we call the Network Informed Restricted Vector Autoregression (NIRVAR) model, yields a coefficient matrix that has a sparse block-diagonal structure. We propose an estimation procedure that embeds each panel component in a low-dimensional latent space and clusters the embedded points to recover the blocks of the coefficient matrix. Crucially, the method allows for network-based time series modelling when the underlying network is unobserved. We derive the bias, consistency and asymptotic normality of the NIRVAR estimator. Simulation studies suggest that the NIRVAR estimated embedded points are Gaussian distributed around the ground truth latent positions. On three applications to finance, macroeconomics, and transportation systems, NIRVAR outperforms competing factor and network time series models in terms of out-of-sample prediction.

Keywords — random graphs, multivariate time series, spectral embedding, stochastic blockmodel.

1 Introduction

Panels of stochastic processes, $\{(X_{1,t}, \dots, X_{N,t})'\}_{t \in \mathbb{Z}}$, which exhibit co-movements between components are central to many scientific disciplines such as environmental science, econometrics, and neuroscience. Often, $X_{i,t}$ depends not only on its own past values, but also on the past values of a subset of other panel components, written $\{X_{j,s} : j \subseteq \{1, \dots, N\}, s < t\}$. For large N , modelling via the time series vector autoregression (VAR) framework becomes prohibitive as the number of model parameters grows as $O(N^2)$ and can quickly exceed the number of observations. Techniques from high-dimensional statistics that introduce some form of sparsity or dimensionality reduction are therefore required in this setting.

Many variants of the factor modelling approach of [Stock and Watson \(2002\)](#) where the large panel of time series are modelled as stemming from a relatively small number of common latent factors have been proposed in statistics and econometrics (see, for example, [Bai, 2003](#); [Fan et al., 2013](#)). Sparse regression methods using various regularised estimation procedures have also been proposed as a way to reduce the number of model parameters. Common methods are the Least Absolute Shrinkage and Selection Operator (LASSO; [Tibshirani, 1996](#)), Smoothly Clipped Absolute Deviation (SCAD; [Fan and Li, 2001](#)), and Least Angle Regression (LARS; [Efron et al., 2004](#)).

Corresponding author: Brendan Martin – ✉ b.martin22@imperial.ac.uk

Network time series approaches in which each univariate time series is observed on a vertex of a graph are also popular in the literature (see, for example [Dahlhaus, 2000](#); [Eichler, 2007](#); [Ahelegbey et al., 2016](#)). The graph can be observed or inferred from data, with the edges of the graph encoding the co-dependence structure of the multivariate time series. For example, [Zhu et al. \(2020\)](#) utilise an observed graph to model the multivariate time series, whereas [Wu et al. \(2020\)](#) infer the underlying graph via a graph neural network. Often, each edge corresponds to a parameter in the time series model. Therefore, if the graph is sparse, the number of model parameters can be smaller than the number of observations, enabling estimation. The estimated parameters can then be used for prediction. In the case that it is inferred from data, the graph itself is of interest for tasks such as clustering, link prediction, and estimation of the Granger causal linkages between panel components ([Lancichinetti and Fortunato, 2009](#); [Zhang and Chen, 2018](#); [Shojaie and Fox, 2022](#)).

This paper proposes a method for inferring a graph structure from multivariate time series data and using it to impose restrictions on the coefficient matrix of a VAR model. Since the network determines the restricted VAR, we call the model the Network Informed Restricted VAR (NIRVAR) model. There is an extensive literature on incorporating network effects into a VAR modelling framework. [Zhu et al. \(2017\)](#) and [Knight et al. \(2016\)](#) independently propose a VAR model in which the network effect on a panel component is the average of its connected neighbours in an observed network. [Knight et al. \(2020\)](#) propose a Generalised Network Autoregressive (GNAR) model which allows for a time-varying observed network, and they show the consistency of generalised least squares estimation of the model parameters. [Fan et al. \(2023\)](#) combine the dimensionality reduction of factor modelling with the parsimony of sparse linear regression and develop a hypothesis testing framework to determine the partial covariance structure. [Barigozzi et al. \(2023\)](#) extend this approach to the setting of dynamic factors, and propose an L_1 -regularised Yule-Walker method for estimating a factor adjusted, idiosyncratic VAR model. The estimated VAR coefficients are then used for network estimation. [Chen et al. \(2023\)](#) introduce a network VAR model that is similar to that of [Zhu et al. \(2017\)](#) but allows for network effects between groups of panel components. They assume that the network adjacency matrix is observable and generated by a stochastic block model (SBM; [Holland et al., 1983](#)). [Guðmundsson and Brownlees \(2021\)](#) introduce a stochastic block VAR model in which the time series are partitioned into latent groups such that the spillover effects are determined by a SBM. A group detection algorithm is developed in which the VAR coefficients are estimated using ordinary least squares (OLS) and used to obtain an embedding on which K -means clustering can be applied.

The method we propose differs from existing works as it involves firstly detecting latent groups from a latent space representation of each time series, and secondly estimating the VAR coefficients. Carrying out estimation in this order is a key contribution of this paper. We avoid estimating a dense VAR parameter matrix as in [Guðmundsson and Brownlees \(2021\)](#) or specifying tuning and thresholding parameters as in [Barigozzi et al. \(2023\)](#). We also emphasise that, in contrast to [Zhu et al. \(2017\)](#), [Knight et al. \(2020\)](#), [Chen et al. \(2023\)](#) and [Barigozzi et al. \(2022\)](#), the NIRVAR estimator does not require the underlying network to be observable, which is a realistic setting in many real-world applications.

NIRVAR models a panel of multivariate time series as a VAR(1) in which the VAR coefficient matrix Φ is the weighted adjacency matrix of some random graph, $\mathcal{G} = (\mathcal{V}, \mathcal{E})$, where each of the N vertexes in the node set \mathcal{V} has an associated d -dimensional latent position $\theta_i \in \mathcal{H}$, $i \in \mathcal{V}$, with $\mathcal{H} \subseteq \mathbb{R}^d$ being some latent space, and where $\mathcal{E} \subseteq \mathcal{V} \times \mathcal{V}$ is a set of random edges. In particular, we model \mathcal{G} as a stochastic block model. Typically, in the random graphs literature, the latent positions are estimated through spectral embedding of the observed adjacency matrix. However, in the settings we consider, the realised graph and its adjacency matrix are unobserved. It is therefore necessary to construct latent positions directly from the observed time series rather than from an observed adjacency matrix. Once latent positions have been constructed, they are clustered into K communities and these communities are used to enforce zero constraints on the VAR coefficients. In particular, if the constructed latent positions of two panel components i and j belong to different clusters, then Φ_{ij} is set to 0. A VAR model with such zero constraints is called a subset VAR model ([Lütkepohl, 2005](#)). The remaining unrestricted parameters are estimated via OLS.

The NIRVAR estimation procedure draws inspiration from the workflow rationalised in [Whiteley et al. \(2022\)](#): linear dimension reduction via principal component analysis, embedding, clustering and graph construction. In particular, we compute the singular value decomposition (SVD) of concatenated sample covariance matrices, con-

sider the corresponding left singular vectors embedding, and cluster the embedded points via a Gaussian mixture model with K components. The embedding dimension is chosen as the number of eigenvalues of the sample covariance matrix that are larger than the upper bound of the support of the Marčenko-Pastur distribution (Marčenko and Pastur, 1967). The motivation for this approach is that large eigenvalues that lie beyond the right edge of the Marčenko-Pastur spectrum are deemed significant and correspond to informative eigenvectors, while eigenvalues below the right edge of the spectrum correspond to noisy eigenvectors. A graph with K cliques is then constructed based on a binary allocation of each embedded point to its most probable Gaussian mixture component. The estimated communities are reconstructions of the blocks of the SBM. The NIRVAR estimator assumes that the probability $p^{(\text{in})}$ of an edge forming within a block is 1, and the probability $p^{(\text{out})}$ of an edge forming between blocks is 0. If $p^{(\text{out})} > p^{(\text{in})}$, the data generating SBM will have a large proportion of inter-block edges and the NIRVAR estimation framework will not capture any of these edges. We therefore restrict our attention to assortative SBMs (see Lee and Wilkinson, 2019, for a review of SBMs). Since the NIRVAR estimator does not recover edges between vertices in different blocks of the data generating SBM, the OLS estimator of the unrestricted VAR parameters will be biased whenever such inter-block edges are present. We derive the bias and show that the NIRVAR estimator is consistent and asymptotically normal.

Each step of the NIRVAR estimation framework can be modified easily. For example, we also consider embedding via the SVD of the precision matrix. Although we do not pursue it here, one could imagine choosing the embedding dimension using, for example, the profile likelihood method of Zhu and Ghodsi (2006) or the ScreeNOT method of Donoho et al. (2023). The motivation for using a Gaussian mixture model instead of say, K -means clustering, is due to the literature on random dot product graphs (Rubin-Delanchy et al., 2022) which shows that spectral embedding yields uniformly consistent latent position estimates with asymptotically Gaussian error (up to identifiability).

NIRVAR can model data that is represented on a multiplex network. A multiplex network is one that has multiple types of edges, with the corresponding graph \mathcal{G} containing multiple layers of connectivity, one layer for each type of edge (De Domenico et al., 2013). If there are Q layers, then the time series data we consider consists of NQ univariate series, $\{X_{i,t}^{(q)}\}_{t \in \mathbb{Z}}$, where $q \in \{1, \dots, Q\}$. In this paper, we refer to the q -th layer as the q -th feature of the matrix time series. These types of matrix time series have been considered by Chang et al. (2023), for example, who propose a one-pass estimation procedure for a tensor canonical polyadic decomposition model of the matrix time series. Barigozzi et al. (2022) also employ a tensor-based principal component approach to a factor network autoregressive model. In contrast, to obtain latent embeddings in the case of multiple features, we unfold the tensor and compute the SVD of $S = (S^{(1)} | \dots | S^{(q)})$ where $S^{(q)}$ is the sample covariance matrix across feature q and $|\dots|$ denotes column concatenation. This choice is motivated by the stability properties of the unfolded adjacency spectral embedding procedure from Gallagher et al. (2021).

The rest of the paper is organised as follows. Section 2 defines the NIRVAR model, outlines the proposed estimation method, and discusses alternative embedding methods. Additionally, we link the NIRVAR model and its corresponding estimator to the literature on spectral embedding of weighted stochastic block models. In Section 3, we derive the bias of the NIRVAR estimator and determine the conditions for which it is unbiased. Furthermore, we show the consistency and asymptotic normality of the estimator and compare its asymptotic efficiency with that of a restricted VAR least-squares estimator with known restrictions. In Section 4, a simulation study is conducted to compare the large sample distribution of NIRVAR parameter estimates with the asymptotic results derived in Section 3 and we also investigate how NIRVAR cluster recovery and parameter estimates vary with different model hyperparameters. Furthermore, we compare the empirical distribution of the NIRVAR estimated embedded points with the ground truth latent positions. In Section 5, we apply NIRVAR to the prediction of financial returns of a universe of US assets, the prediction of US industrial production, and the prediction of daily bicycle rides from Santander stations in London, and conclude that NIRVAR obtains the best performance across all data sets and tasks. The data and code are available in the Github repository [bmartin9/NIRVAR](https://github.com/bmartin9/NIRVAR).

1.1 Notation

For an integer k , let $[k]$ denote the set $\{1, \dots, k\}$. The $n \times n$ identity matrix is written I_n , and the indicator function is $\mathbb{1}\{\mathcal{B}\} = 1$ if the event \mathcal{B} occurs and 0 otherwise. For vectors, $v_1, \dots, v_n \in \mathbb{R}^p$, let $M = (v_1, \dots, v_n) \in \mathbb{R}^{p \times n}$

be the matrix whose columns are given by $\mathbf{v}_1, \dots, \mathbf{v}_n$. The column space of M is $\text{colsp}(M)$, its rank is $\text{rk}(M)$, and its transpose is M' . We write $M_{i,\cdot}$ and $M_{\cdot,j}$ to denote the i -th row and j -th column of M considered as vectors, respectively. The element-wise ℓ_0 norm is defined as $|M|_0 = \sum_{i=1}^p \sum_{j=1}^n \mathbb{1}\{M_{ij} \neq 0\}$. The Frobenius norm is $\|M\|_F = (\sum_{i=1}^p \sum_{j=1}^n |M_{ij}|^2)^{1/2}$. The spectral radius of an $n \times n$ matrix A is $\rho(A) = \max\{|\lambda_1|, \dots, |\lambda_n|\}$ where $\lambda_1, \dots, \lambda_n$ are the eigenvalues of A . The vectorisation operator $\text{vec}(\cdot)$ transforms a $p \times n$ matrix M into a $pn \times 1$ vector by stacking its columns. Let \odot denote the Hadamard product between two matrices of the same dimensions, and \otimes denote the Kronecker product between two matrices, not necessarily of the same dimension. For matrices M_1, \dots, M_r , let $(M_1 | \dots | M_r)$ and $(M_1; \dots; M_r)$ denote the column-wise and row-wise concatenation of the matrices, respectively. The set of $n \times d$ matrices with orthogonal columns is $\mathbb{O}(n \times d)$. For a distribution F the support of F is $\text{supp}(F)$.

2 Model and Estimation

2.1 Model

Let $\mathbf{X}_t = (X_{i,t}^{(q)})$ be a matrix consisting of NQ random variables at each time $t \in \mathbb{Z}$. For example, $i \in [N]$ could label an individual and $q \in [Q]$ a particular variable or feature associated with that individual. Consider an associated multiplex network with Q layers each having N vertices. The random variable $X_{i,t}^{(q)}$ is observed at vertex i of layer q of the multiplex network. A feature is then just a layer of the multiplex network. For each feature $q \in [Q]$ we associate a random graph $\mathcal{G}^{(q)} = (\mathcal{V}, \mathcal{E}^{(q)})$ where $\mathcal{V} = [N]$. $\mathcal{G}^{(q)}$ is modelled as a SBM. We utilise the random dot product graph (RDPG; Athreya et al., 2017) representation of the SBM since our subsequent estimation method involves constructing latent positions for each node, which are then clustered in order to recover the blocks of the SBM, providing a convenient mathematical framework.

Definition 2.1 (Directed RDPG with distribution F and self-loops). *Let F be a d -dimensional distribution with support $\text{supp}(F) = \mathcal{H} \subset \mathbb{R}^d$, such that $\mathbf{x}'\mathbf{y} \in [0, 1]$ for all $\mathbf{x}, \mathbf{y} \in \mathcal{H}$. F is also known as inner product distribution (Athreya et al., 2021). Also, let $\boldsymbol{\theta}_1, \dots, \boldsymbol{\theta}_N \sim F$ collected in the rows of the matrix $\Theta = (\boldsymbol{\theta}_1, \dots, \boldsymbol{\theta}_N)' \in \mathbb{R}^{N \times d}$. Suppose A is a random adjacency matrix such that, conditional on Θ :*

$$p(A | \Theta) = \prod_{i=1}^N \prod_{\substack{j=1 \\ j \neq i}}^N (\boldsymbol{\theta}'_i \boldsymbol{\theta}_j)^{A_{ij}} (1 - \boldsymbol{\theta}'_i \boldsymbol{\theta}_j)^{1-A_{ij}} \prod_{h=1}^N \mathbb{1}\{A_{hh} = 1\},$$

where $p(\cdot)$ represents a probability mass function. Then we say that A is the adjacency matrix of a directed RDPG with self-loops of rank at most d and with latent positions given by the rows of Θ , written $(A, \Theta) \sim \text{RDPG}(F)$.

Remark 1. *In contrast to the definition given by Athreya et al. (2017), Definition 2.1 does not restrict A to be symmetric and have all of the principal diagonal elements equal to zero. This is to allow for directed graphs with self loops. With a slight abuse of notation, RDPG will be used in the rest of this work to denote a directed random dot product graph with self-loops.*

Definition 2.2 (K -block SBM). *We say that $(A, \Theta) \sim \text{RDPG}(F)$ is a SBM with K blocks or communities if the number of distinct rows in Θ is K . We define the block membership function $z : [N] \mapsto [K]$ to be a function such that $z_i = z_j$ if and only if $\boldsymbol{\theta}_i = \boldsymbol{\theta}_j$ (where $z(i) \equiv z_i$). Under this representation, $F(\boldsymbol{\theta}) = \sum_{k=1}^K \pi_k \delta(\boldsymbol{\theta} - \boldsymbol{\nu}_k)$, where $\boldsymbol{\nu}_k \in \mathbb{R}^d, k \in [K]$ are community-specific latent positions chosen such that $\boldsymbol{\nu}'_k \boldsymbol{\nu}_\ell \in [0, 1]$ for all $k, \ell \in [K]$, and $\pi = (\pi_1, \dots, \pi_K)$ represent the prior probabilities of each node to belong to the k -th community, with $\pi_k \geq 0$ for all $k \in [K]$ and $\sum_{k=1}^K \pi_k = 1$. Here, δ is the d -dimensional Dirac delta function. The between-community connection probabilities can be collected in a matrix $B \in [0, 1]^{K \times K}$ with $B_{k\ell} = \boldsymbol{\nu}'_k \boldsymbol{\nu}_\ell, \boldsymbol{\nu}_k, \boldsymbol{\nu}_\ell \in \mathbb{R}^d$ for $k, \ell = 1, \dots, K$, and we write $(A, \Theta) \sim \text{SBM}(B, \pi)$.*

Note that Definition 2.2 only covers the case in which the matrix $B \in [0, 1]^{K \times K}$ of between-block connection probabilities is positive semi-definite. In our work, we assume that the graph is assortative, corresponding to the

case of a positive semi-definite matrix B . The motivation for this assumption is to have a multivariate time series model in which there is greater co-movement between panel components within the same community than between communities. The generalised RDPG (Rubin-Delanchy et al., 2022) provides an extension to the indefinite case.

In the NIRVAR model, it is assumed that each feature-specific graph $\mathcal{G}^{(q)} = (\mathcal{V}, \mathcal{E}^{(q)})$ with adjacency matrix $A^{(q)}$ has an associated latent position matrix $\Theta^{(q)}$ such that

$$(A^{(q)}, \Theta^{(q)}) \sim \text{SBM}(B^{(q)}, \pi^{(q)}), \quad q = 1, \dots, Q,$$

where $B^{(q)} \in [0, 1]^{K \times K}$ and $\pi^{(q)}$ are feature-specific SBM parameters. The probability of an edge forming between vertices i and j , $i \neq j$, is

$$p_{ij}^{(q)} = B_{z_i z_j} = \theta_i^{(q)'} \theta_j^{(q)},$$

and the adjacency matrix corresponding to $\mathcal{G}^{(q)}$ is

$$A_{ij}^{(q)} \sim \text{Bernoulli}(p_{ij}^{(q)}). \quad (1)$$

Given $\mathcal{G}^{(q)}$, we define the NIRVAR model as follows.

Definition 2.3 (NIRVAR model). *For some fixed $q \in [Q]$, let $\{\mathbf{X}_t^{(q)}\}_{t \in \mathbb{Z}}$ denote a zero mean, second order stationary stochastic process where $\mathbf{X}_t^{(q)} = (X_{1,t}^{(q)}, \dots, X_{N,t}^{(q)})' \in \mathbb{R}^N$ and $q \in [Q]$. The NIRVAR model for the q -th feature is*

$$\mathbf{X}_t^{(q)} = \sum_{r=1}^Q (A_q^{(r)} \odot \tilde{\Phi}_q^{(r)}) \mathbf{X}_{t-1}^{(r)} + \boldsymbol{\epsilon}_t^{(q)}, \quad \boldsymbol{\epsilon}_t^{(q)} \sim \mathcal{N}(0, \Sigma), \quad (2)$$

in which the generic element of $A_q^{(r)}$, $r \in [Q]$ is given by Equation (1) and $\tilde{\Phi}_q^{(r)}$, $r \in [Q]$ is an $N \times N$ matrix of fixed weights. The covariance matrix of the noise process, Σ , is assumed to be positive definite. Defining $\Phi_q^{(r)} := A_q^{(r)} \odot \tilde{\Phi}_q^{(r)}$ and $\Phi_q := (\Phi_q^{(1)} | \dots | \Phi_q^{(Q)})$, we write $\mathbf{X}_t^{(q)} \sim \text{NIRVAR}(\Phi_q)$.

If, for each $q \in [Q]$, $\mathbf{X}_t^{(q)} \sim \text{NIRVAR}(\Phi_q)$, then $Z_t := (\mathbf{X}_t^{(1)'}, \dots, \mathbf{X}_t^{(Q)'})' \in \mathbb{R}^{NQ}$ is a VAR(1) process with coefficient matrix $\Xi := (\Phi_1; \dots; \Phi_Q) \in \mathbb{R}^{NQ \times NQ}$. Therefore, $\mathbf{X}_t^{(q)}$ will be stable, and hence stationary, if $\rho(\Xi) < 1$ (Lütkepohl, 2005).

Remark 2. *In Equation (2) in Definition 2.3, we define the NIRVAR model only for the q -th feature, which acts as the response or endogenous variable, whereas the features $\mathcal{C}_{-q} = [Q] \setminus \{q\}$ are interpreted as covariates or exogenous variables. Since we focus on the response of the q -th feature, we drop the subscript on $A_q^{(r)}$, $\tilde{\Phi}_q^{(r)}$, $\Phi_q^{(r)}$, and Φ_q for the remainder of the paper.*

It will be convenient when discussing estimation of the NIRVAR model to write Equation (2) in vectorised form. For this purpose, we define

$$\Psi^{(q)} := (\mathbf{X}_1^{(q)}, \dots, \mathbf{X}_T^{(q)}), \quad Z := (Z_0, \dots, Z_{T-1}), \quad U^{(q)} := (\boldsymbol{\epsilon}_1^{(q)}, \dots, \boldsymbol{\epsilon}_T^{(q)}), \quad A := (A^{(1)} | \dots | A^{(Q)}).$$

We can then write Equation (2) for $t = 1, \dots, T$ as

$$\Psi^{(q)} = \Phi Z + U^{(q)},$$

or, in vectorised form,

$$\boldsymbol{\psi}^{(q)} = \text{vec}(\Phi Z) + \text{vec}(U^{(q)}) = (Z' \otimes I_N) \boldsymbol{\beta} + \mathbf{u}^{(q)}, \quad (3)$$

where we define $\boldsymbol{\psi}^{(q)} := \text{vec}(\Psi^{(q)})$, $\boldsymbol{\beta} := \text{vec}(\Phi)$, and $\mathbf{u}^{(q)} := \text{vec}(U^{(q)})$. The number of non-zero elements of $\boldsymbol{\beta}$ is given by $M = |A|_0$.

The model can be written in terms of an unrestricted M -dimensional vector $\gamma(A)$ whose elements are those in the set $\{\beta_i : \text{vec}(A)_i \neq 0, i = 1, \dots, N^2Q\}$. Additionally, an $N^2Q \times M$ matrix $R(A)$ is defined via the mapping $R : \{0, 1\}^{N \times NQ} \rightarrow \{0, 1\}^{N^2Q \times M}$, where

$$[R(A)]_{ij} := \text{vec}(A)_i \times \mathbb{1} \left\{ \sum_{k=1}^{i-1} \text{vec}(A)_k = j - 1 \right\}. \quad (4)$$

The constraints on β can then be written as

$$\beta = R(A)\gamma(A). \quad (5)$$

Combining Equation (3) and Equation (5) finally yields

$$\psi^{(q)} = (Z' \otimes I_N) R(A)\gamma(A) + \mathbf{u}^{(q)}. \quad (6)$$

2.2 Estimation

The NIRVAR estimation method proceeds by firstly imposing subset VAR restrictions through a binary matrix, $\hat{A} \in \{0, 1\}^{N \times NQ}$, and then estimating $\gamma(\hat{A})$. To obtain \hat{A} , a low-dimensional latent representation of each panel component is found by embedding the sample covariance matrix in some latent space. Clustering the latent positions then allows for the construction of a graph with adjacency matrix \hat{A} .

The embedding and clustering method used here follows the workflow suggested by [Whiteley et al. \(2022\)](#) who propose a statistical model called the latent metric model to explain the manifold hypothesis. The manifold hypothesis posits that many high-dimensional data sets are in fact samples from a lower-dimensional manifold ([Cayton et al., 2008](#)). [Whiteley et al. \(2022\)](#) give theoretical justification for the commonly employed approach of linear dimensionality reduction via principal component analysis, a subsequent embedding, and graph construction using the embedded points. The next sections describe these steps in details.

2.2.1 Embedding

Let $X^{(q)} = (\mathbf{x}_1^{(q)}, \dots, \mathbf{x}_T^{(q)})$ be the $N \times T$ design matrix of feature q where $\mathbf{x}_t^{(q)} = (x_{1,t}^{(q)}, \dots, x_{N,t}^{(q)})'$ is a realisation of the random variable $\mathbf{X}_t^{(q)}$. To construct an embedding $\hat{\mathbf{y}}_i^{(q)} \in \mathbb{R}^d$ we are motivated by the unfolded adjacency spectral embedding of [Jones and Rubin-Delanchy \(2020\)](#), which obtains embeddings $Y^{(q)} \in \mathbb{R}^{N \times d}$ by considering the SVD of $A = (A^{(1)} | \dots | A^{(Q)})$. Unfolded adjacency spectral embedding has two key stability properties shown by [Gallagher et al. \(2021\)](#): it assigns the same position, up to noise, to vertices behaving similarly for a given feature (cross-sectional stability) and a constant position, up to noise, to a single vertex behaving similarly across different features (longitudinal stability). Since we do not observe $A^{(q)}$, we instead consider the SVD of $S = (S^{(1)} | \dots | S^{(Q)}) \in \mathbb{R}^{N \times NQ}$ where $S^{(q)} := X^{(q)} X^{(q)'} / T \in \mathbb{R}^{N \times N}$ is the sample covariance matrix for feature q . We can write S as

$$S = UDV' + U_{\perp} D_{\perp} V'_{\perp},$$

where $D \in \mathbb{R}^{d \times d}$ is a diagonal matrix containing the d largest singular values of S , and the columns of $U \in \mathbb{O}(N \times d)$ and $V \in \mathbb{O}(NQ \times d)$ are the corresponding d left and right singular vectors, respectively. The choice of d is discussed below. Assuming S admits a low-rank approximation, unfolded adjacency spectral embedding uses only $\hat{S} = UDV'$ to produce embeddings. In particular, the q -th right unfolded adjacency spectral embedding is the matrix $\hat{Y}^{(q)} \in \mathbb{R}^{N \times d}$ obtained by dividing $\hat{Y} = VD^{1/2} \in \mathbb{R}^{NQ \times d}$ into Q equal blocks, $\hat{Y} = (\hat{Y}^{(1)}; \dots; \hat{Y}^{(Q)})$. The feature- q embedding of time series i is thus $\hat{\mathbf{y}}_i^{(q)} = (\hat{Y}^{(q)})_{i,:}$.

It is of interest to relate $\hat{\mathbf{y}}_i^{(q)}$ to the ground truth latent positions $\theta_i^{(q)}$, since clustering of $\hat{\mathbf{y}}_i^{(q)}$ will be used to recover the blocks of the data generating SBM. We derive a connection between the covariance matrix $\Gamma^{(q)} = \mathbb{E}\{(\mathbf{X}_t^{(q)})(\mathbf{X}_t^{(q)})'\}$ of a NIRVAR(Φ) process and $\theta_i^{(q)}$ for the case $Q = 1$. Under a technical assumption of symmetric Φ , Proposition 2.4 shows that the rank d spectral embedding of $\Gamma^{(q)}$ and Φ are equivalent. Since we assume $Q = 1$ in Proposition 2.4, the superscript q is dropped for readability.

Proposition 2.4. Let $\mathbf{X}_t \sim \text{NIRVAR}(\Phi)$ where Φ is assumed to be symmetric. Consider the eigendecomposition

$$\Phi = U_\Phi \Lambda_\Phi U_\Phi' + U_{\Phi,\perp} \Lambda_{\Phi,\perp} U_{\Phi,\perp}'$$

where $U_\Phi \in \mathbb{O}(N \times d)$ and Λ_Φ is a $d \times d$ diagonal matrix comprising the d largest eigenvalues in absolute value of Φ . Then the rank d truncated eigendecomposition of the covariance matrix $\Gamma = \mathbb{E}(\mathbf{X}_t \mathbf{X}_t')$ is $\Gamma = U_\Gamma \Lambda_\Gamma U_\Gamma'$ in which Λ_Γ is a $d \times d$ diagonal matrix with diagonal elements $(\lambda_\Gamma)_i = 1/\{1 - (\lambda_\Phi)_i^2\}$ where $(\lambda_\Phi)_i$ is the corresponding diagonal entry of Λ_Φ .

The proof of Proposition 2.4 is in Appendix A.1 of the online supplementary material.

Under the assumptions of Proposition 2.4, the eigenvectors corresponding to the d largest eigenvalues of Γ and Φ are the same. Therefore, the rank d spectral embedding of Φ can be constructed, up to identifiability, from the eigenvectors and scaled eigenvalues of Γ , where the scaling is given by $(\lambda_\Phi)_i = \pm\sqrt{1 - 1/(\lambda_\Gamma)_i}$.

For the case where Φ is symmetric, Gallagher et al. (2023) prove a central limit theorem for the asymptotic behaviour of $Y_\Phi = U_\Phi \Lambda_\Phi^{1/2}$. They prove that, up to a sequence of orthogonal transformations, $(Y_\Phi)_i$ is asymptotically normally distributed around the ground truth latent positions, θ_i . The relation between $Y_\Gamma = U_\Gamma \Lambda_\Gamma^{1/2}$ and Y_Φ shown by Proposition 2.4 suggests that there may be a similar connection between $(Y_\Gamma)_i$ and θ_i . A simulation study comparing $(Y_\Gamma)_i$ and θ_i is discussed in Section 4.

2.2.2 Clustering

Clustering via a Gaussian mixture model can be used to assign a label $\hat{z}_i^{(q)} \in \{1, \dots, K\}$ to each panel component based on $\hat{\mathbf{y}}_i^{(q)}$. In particular, we use Expectation-Maximisation (Dempster et al., 1977) to maximise the Gaussian mixture model incomplete log-likelihood and estimate the cluster assignments $\hat{z}_i^{(q)}$. We define $\hat{A} = (\hat{A}^{(1)} | \dots | \hat{A}^{(Q)}) \in \{0, 1\}^{N \times NQ}$ as

$$\hat{A}_{ij}^{(q)} = \mathbb{1} \left\{ \hat{z}_j^{(q)} = \hat{z}_i^{(q)} \right\}.$$

From this definition, it can be seen that \hat{A} defines a graph with K cliques and therefore cannot recover inter-block edges of the data generating SBM.

We use the following argument to motivate our choice of K . For a RDPG, $A_{ij}^{(q)} \sim \text{Bernoulli}(\theta_i^{(q)'} \theta_j^{(q)})$ and thus $\mathbb{E}(A^{(q)}) = \Theta^{(q)} \Theta^{(q)'}$, where $\Theta^{(q)} = (\theta_1^{(q)}, \dots, \theta_N^{(q)})' \in \mathbb{R}^{N \times d}$. Assuming that $\Theta^{(q)}$ is full rank, then $\text{rank}\{\mathbb{E}(A^{(q)})\} = \text{rank}(\Theta^{(q)} \Theta^{(q)'}) = \text{rank}(\Theta^{(q)}) = d$. Now for a SBM, $\Theta^{(q)}$ has K distinct rows (corresponding to the K latent positions), and thus $\text{rank}(\Theta^{(q)}) = K$. Since we are assuming $\mathcal{G}^{(q)}$ is a SBM, we set $K = d$.

2.2.3 OLS estimation of VAR coefficients

The subset VAR restrictions we impose correspond to the zero entries of \hat{A} . Given \hat{A} , there are $\widehat{M} = |\hat{A}|_0$ remaining unrestricted parameters that we estimate via OLS. Let $\gamma(\hat{A})$ be the \widehat{M} -dimensional vector of unrestricted parameters whose elements are those in the set $\{\beta_i : \text{vec}(\hat{A})_i \neq 0, i = 1, \dots, N^2Q\}$. Let $R(\hat{A}) \in \{0, 1\}^{N^2Q \times \widehat{M}}$ be the restrictions matrix corresponding to \hat{A} where R is defined by Equation (4). The model corresponding to the estimated restrictions \hat{A} is

$$\psi_{\hat{A}}^{(q)} = (Z' \otimes I_N) R(\hat{A}) \gamma(\hat{A}) + \mathbf{u}^{(q)}. \quad (7)$$

Comparing with Equation (6), we see that Equation (7) will be misspecified if $\text{vec}(\hat{A})_i = 0$ but $\text{vec}(A)_i = 1$ for any $i = 1, \dots, NQ$. In this case, $\psi_{\hat{A}}^{(q)} \neq \psi^{(q)}$. Following Lütkepohl (2005, Section 3.2.1), we look for the estimator of $\gamma(\hat{A})$ that minimises the objective

$$S\{\gamma(\hat{A})\} = \{\psi^{(q)} - (Z' \otimes I_N) R(\hat{A}) \gamma(\hat{A})\}' (I_T \otimes \Sigma^{-1}) \{\psi^{(q)} - (Z' \otimes I_N) R(\hat{A}) \gamma(\hat{A})\}$$

$$= \boldsymbol{\psi}^{(q)'}(I_T \otimes \Sigma^{-1})\boldsymbol{\psi}^{(q)} + \boldsymbol{\gamma}(\hat{A})'R(\hat{A})'(ZZ' \otimes \Sigma^{-1})R(\hat{A})\boldsymbol{\gamma}(\hat{A}) - 2\boldsymbol{\gamma}(\hat{A})'R(\hat{A})'(Z \otimes \Sigma^{-1})\boldsymbol{\psi}^{(q)}.$$

Hence,

$$\frac{\partial S\{\boldsymbol{\gamma}(\hat{A})\}}{\partial \boldsymbol{\gamma}(\hat{A})} = 2R(\hat{A})'(ZZ' \otimes \Sigma^{-1})R(\hat{A})\boldsymbol{\gamma}(\hat{A}) - 2R(\hat{A})'(Z \otimes \Sigma^{-1})\boldsymbol{\psi}^{(q)}.$$

Equating to zero yields the generalised least-squares estimator

$$\hat{\boldsymbol{\gamma}}(\hat{A}) = \{R(\hat{A})'(ZZ' \otimes \Sigma^{-1})R(\hat{A})\}^{-1}R(\hat{A})'(Z \otimes \Sigma^{-1})\boldsymbol{\psi}^{(q)}. \quad (8)$$

For the simulation studies in Section 4 and applications in Section 5, we assume that $\Sigma = \sigma^2 I_N$, in which case the generalised least-squares estimator is the same as the multivariate least-squares estimator

$$\hat{\boldsymbol{\gamma}}(\hat{A}) = \{R(\hat{A})'(ZZ' \otimes I_N)R(\hat{A})\}^{-1}R(\hat{A})'(Z \otimes I_N)\boldsymbol{\psi}^{(q)}.$$

Finally, the least-squares estimator of $\boldsymbol{\beta}$ is

$$\hat{\boldsymbol{\beta}}(\hat{A}) = R(\hat{A})\hat{\boldsymbol{\gamma}}(\hat{A}). \quad (9)$$

2.2.4 Determining the embedding dimension

We employ tools from random matrix theory to estimate $d^{(q)}$, the rank of the RDPG $\mathcal{G}^{(q)}$. Following standard methods in the literature (see, for example [Laloux et al., 2000](#)), our estimate $\hat{d}^{(q)}$ is the number of eigenvalues of $S^{(q)}$ that are larger than the upper bound of the support of the Marčenko-Pastur distribution ([Marčenko and Pastur, 1967](#)). The Marčenko-Pastur distribution is the limiting eigenvalue distribution of an $N \times N$ Wishart matrix whose dimension to sample size ratio is a constant, $\eta = N/T$, and is given by

$$f_{\text{MP}}(x; \eta, \sigma^2) = \begin{cases} \sqrt{(x - x_-)(x_+ - x)}/(2\pi\sigma^2\eta) & \text{if } x_- \leq x \leq x_+, \\ 0 & \text{otherwise,} \end{cases}$$

with σ^2 being the scale parameter and $x_{\pm} = \sigma^2(1 \pm \sqrt{\eta})^2$ (for a derivation, see [Bai and Silverstein, 2010](#)). If $\lambda_1^{(q)}, \dots, \lambda_N^{(q)}$ are the eigenvalues of $S^{(q)}$, then

$$\hat{d}^{(q)} = \sum_{j=1}^N \mathbb{1}\{\lambda_j^{(q)} > x_+\}.$$

The interpretation is that all eigenvalues that are greater than x_+ cannot be attributed to random noise and are thus deemed as “informative”.

Another approach to determining the embedding dimension using random matrix theory is to consider the distribution of the largest eigenvalue of a Wishart matrix, which, when centered and scaled, tends towards the Tracy-Widom distribution ([Johnstone, 2001](#)). The 95th percentile of the Tracy-Widom distribution could then be chosen as the cut-off above which eigenvalues of the sample covariance matrix are deemed informative.

2.3 Alternative embeddings

Alternatives to the sample covariance matrix could be chosen for the embedding procedure described in Section 2.2.1. Here, we discuss embedding the precision matrix, $\Omega^{(q)} = (S^{(q)})^{-1}$. One motivation for the use of the precision matrix is its relation to the partial correlation

$$\text{Cor}\left(\Psi_{i,:}^{(q)}, \Psi_{j,:}^{(q)} \mid \Psi_{-(i,j),:}^{(q)}\right) = -\frac{\Omega_{ij}^{(q)}}{\Omega_{ii}^{(q)}\Omega_{jj}^{(q)}},$$

where $\Psi_{-(i,j),:}^{(q)}$ denotes the set of all rows of $\Psi^{(q)}$ except rows i and j . We can thus interpret $\Omega_{ij}^{(q)}$ as being proportional to the remaining correlation between time series i and time series j for feature q after the residual effect of all other time series has been removed. The unfolded adjacency spectral embedding and Gaussian mixture model clustering steps in the estimation procedure remain unchanged using the precision matrix. However, we need to slightly modify our method for estimating $d^{(q)}$. Instead of counting the number of eigenvalues of $S^{(q)}$ that are larger than the upper bound of the support of the Marčenko-Pastur distribution, we count the number of eigenvalues of $\Omega^{(q)}$ that are smaller than the lower bound of the support of the inverse Marčenko-Pastur distribution, which is the distribution of the reciprocal of a Marčenko-Pastur distributed random variable. The inverse Marčenko-Pastur distribution is derived in Appendix A.5 of the online supplementary material and is given by

$$f_{\text{IMP}}(y; \eta, \sigma^2) = \begin{cases} (1 - \eta) \sqrt{(y_+ - y)(y - y_-)} / (2\pi\eta y^2) & \text{if } y_- \leq y \leq y_+, \\ 0 & \text{otherwise,} \end{cases}$$

where

$$y_{\pm} = \frac{1}{\sigma^2} \left(\frac{1 \pm \sqrt{\eta}}{1 - \eta} \right)^2.$$

If $\zeta_1^{(q)}, \dots, \zeta_N^{(q)}$ are the eigenvalues of $\Omega^{(q)}$, then our estimate of $d^{(q)}$ when using the precision matrix becomes

$$\hat{d}^{(q)} = \sum_{j=1}^N \mathbb{1} \left\{ \zeta_j^{(q)} < y_- \right\}.$$

3 Asymptotic Properties

In this section we derive the bias, consistency and asymptotic normality of the NIRVAR generalised least-squares estimator given by Equation (9). We show that it is biased whenever an incorrect restriction is placed on the VAR matrix, that is, whenever $\hat{A}_{ij}^{(q)} = 0$ but $A_{ij}^{(q)} = 1$, and unbiased otherwise. The proof of consistency and asymptotic normality is an extension of the theory of restricted VAR models (see, for example, Chapter 5 of Lütkepohl, 2005) to the case where the restrictions may be misspecified. Furthermore, for the case in which a proper subset of the true restrictions are known, we prove that the asymptotic variance of the corresponding estimator is greater than or equal to that of a restricted estimator that uses all restrictions. Substituting Equation (3) into Equation (8) using Equation (5) yields

$$\begin{aligned} \hat{\gamma}(\hat{A}) &= \{R(\hat{A})'(ZZ' \otimes \Sigma^{-1})R(\hat{A})\}^{-1} R(\hat{A})'(Z \otimes \Sigma^{-1}) \{ (Z' \otimes I_N)R(A)\gamma(A) + \mathbf{u}^{(q)} \} \\ &= \{R(\hat{A})'(ZZ' \otimes \Sigma^{-1})R(\hat{A})\}^{-1} R(\hat{A})'(ZZ' \otimes \Sigma^{-1})R(A)\gamma(A) \\ &\quad + \{R(\hat{A})'(ZZ' \otimes \Sigma^{-1})R(\hat{A})\}^{-1} R(\hat{A})'(I_{NQ} \otimes \Sigma^{-1}) \text{vec}(U^{(q)}Z'). \end{aligned}$$

Noting that $\mathbb{E}\{\text{vec}(U^{(q)}Z')\} = (Z \otimes I_N)\mathbb{E}\{\mathbf{u}^{(q)}\} = 0$, we see that the bias of the estimator, given \hat{A} , is $\mathbb{E}\{\hat{\beta}(\hat{A})|\hat{A}\} = R(\hat{A})C\gamma(A)$, where

$$C := \{R(\hat{A})'(ZZ' \otimes \Sigma^{-1})R(\hat{A})\}^{-1} R(\hat{A})'(ZZ' \otimes \Sigma^{-1})R(A). \quad (10)$$

The following proposition gives the conditions under which $\hat{\beta}(\hat{A})$ is an unbiased estimator of β .

Proposition 3.1. *Conditional on the estimated restrictions \hat{A} , the NIRVAR estimator $\hat{\beta}(\hat{A})$ given by Equation (9) is unbiased if and only if $\text{colsp}\{R(A)\} \subseteq \text{colsp}\{R(\hat{A})\}$, where A specifies the true restrictions and \hat{A} specifies the estimated restrictions.*

The proof of Proposition 3.1 is in Appendix A.2 of the online supplementary material. We now consider the asymptotic properties of $\hat{\gamma}(\hat{A})$.

Proposition 3.2. *The NIRVAR estimator $\hat{\gamma}(\hat{A})$ given by Equation (8) is a consistent estimator of $C\gamma(A)$ where C is defined by Equation (10), and*

$$\sqrt{T} \left\{ \hat{\gamma}(\hat{A}) - C\gamma(A) \right\} \xrightarrow{d} \mathcal{N} \left(0, \left\{ R(\hat{A})' (\Gamma \otimes \Sigma^{-1}) R(\hat{A}) \right\}^{-1} \right), \quad (11)$$

where $\Gamma := \mathbb{E}(Z_t Z_t') = \text{plim } Z Z' / T$.

The proof of Proposition 3.2 is in Appendix A.3 of the online supplementary material. It is informative to compare the asymptotic efficiency of $\hat{\gamma}(A)$ (the generalised least-squares estimator given that the true restrictions are known) with $\hat{\gamma}(\hat{A})$ for the case where $\text{colsp}\{R(A)\} \subseteq \text{colsp}\{R(\hat{A})\}$ (that is, \hat{A} contains no misspecified restriction, but may not include *all* of the true restrictions). The following proposition proves that, in this case, $\hat{\gamma}(A)$ is asymptotically never less efficient than $\hat{\gamma}(\hat{A})$.

Proposition 3.3. *Let $\hat{\beta}(A) = R(A)\hat{\gamma}(A)$ and $\hat{\beta}(\hat{A}) = R(\hat{A})\hat{\gamma}(\hat{A})$ be the generalised least-squares estimators given by Equation (9) for the case where A specifies the true restrictions of the data generating process and \hat{A} is another set of restrictions that satisfies $\text{colsp}\{R(A)\} \subseteq \text{colsp}\{R(\hat{A})\}$. Then the asymptotic variance of $\hat{\beta}(\hat{A})$ is greater than or equal to that of $\hat{\beta}(A)$ in the sense that*

$$\text{var} \left[\sqrt{T} \left\{ \hat{\beta}(\hat{A}) - \beta \right\} \right] - \text{var} \left[\sqrt{T} \left\{ \hat{\beta}(A) - \beta \right\} \right] \succeq 0,$$

where \succeq denotes positive semi-definite.

The proof of Proposition 3.3 is in Appendix A.4 of the online supplementary material.

4 Simulation study

In this section, we conduct an extended simulation study. We simulate the underlying network from a stochastic block model with $B_{kh} = p^{(\text{in})} \in [0, 1]$ for $k = h$ and $B_{kh} = p^{(\text{out})} \in [0, 1]$ for $k \neq h$, $k, h \in [K]$. Firstly, we check whether NIRVAR cluster recovery and parameter estimates improve as the spectral radius of the ground truth VAR coefficient matrix $\rho(\Phi)$ increases. We expect this to be the case since $\rho(\Phi)$ controls the signal-to-noise ratio of the data generating process. Secondly, the ability of the NIRVAR estimator to obtain the correct restrictions should decrease as the number of edges between blocks increases. We thus count the number of errors in \hat{A} as a function of the probability $p^{(\text{out})}$ of an edge forming between blocks in the simulated data generating process. Thirdly, we compare the NIRVAR estimated latent positions with the ground truth latent positions of the data generating SBM. Lastly, the asymptotic distribution given by Proposition 3.2 is compared to the distribution of parameter estimates $\hat{\gamma}(\hat{A})$ obtained from a large finite sample.

4.1 Spectral radius

The hyperparameters used to generate data from the NIRVAR model were $N = 100$, $Q = 1$, $K \in \{2, 10\}$, and $T \in \{250, 500, 750, 1000\}$. To set $\tilde{\Phi}$, we sampled each entry $\tilde{\Phi}_{ij}$ independently from a Uniform(0,1) distribution and then normalised such that $\rho(\Phi)$ was the desired value. The normalised root mean squared error (NRMSE) and Adjusted Rand Index (ARI, [Hubert and Arabie, 1985](#)) for $\rho(\Phi) \in \{0.5, 0.55, 0.6, 0.65, 0.7, 0.75, 0.8, 0.85, 0.9, 0.95\}$ are shown in Figure 1. The ARI is a measure of the similarity between two clusterings of data. It ranges from -1 to 1, with an ARI of 1 indicating a perfect agreement between the two clusterings, 0 indicating a random agreement and -1 indicating that the two clusterings are completely different. For each combination of $\rho(\Phi)$ and T , we sampled $\mathbf{X}_t^{(q)} \sim \text{NIRVAR}(\Phi)$, obtained an estimate $\hat{\Phi}$ of Φ from the simulated data, and computed the NRMSE between $\hat{\Phi}$ and Φ , defined as

$$\text{NRMSE} = \frac{\|\hat{\Phi} - \Phi\|_F}{\hat{M}\rho(\Phi)}.$$

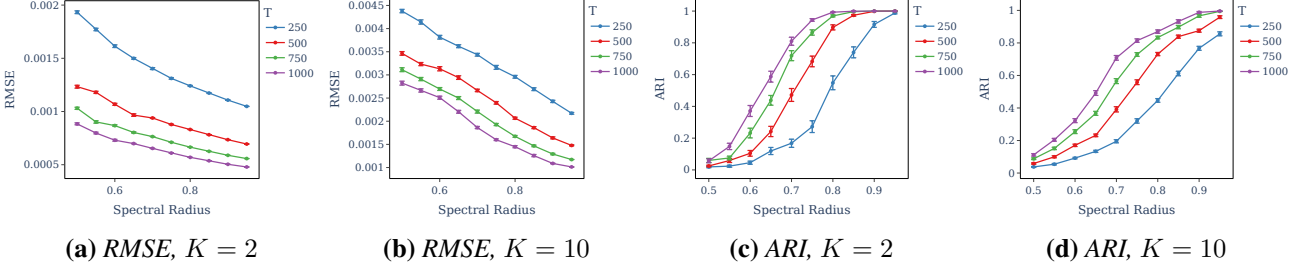


Figure 1: (a)-(b) Comparing the normalised RMSE between the NIRVAR estimated parameters $\hat{\Phi}$ and the simulation study ground truth Φ as the spectral radius $\rho(\Phi)$ is increased. (c)-(d) Comparing the ARI between the NIRVAR estimated clusters and the simulation study ground truth clusters as $\rho(\Phi)$ is increased.

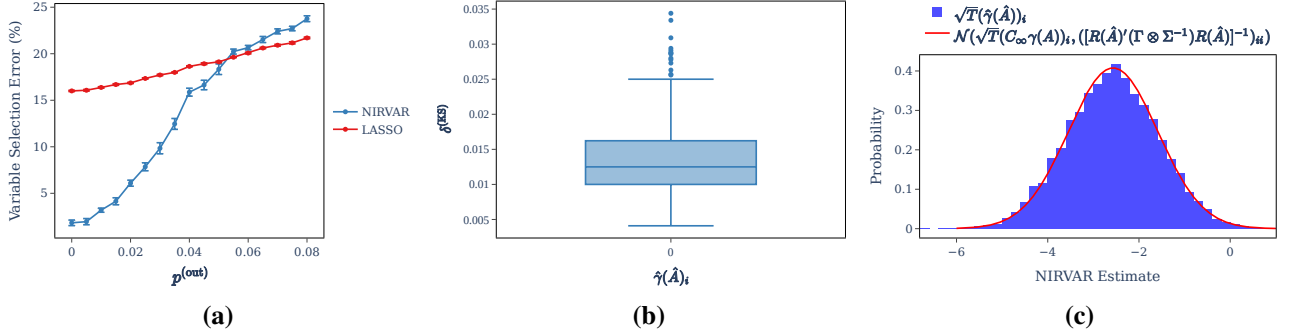


Figure 2: (a) The percentage error in estimated restrictions as $p^{(out)}$ increases. (b) The KS statistic between the empirical distribution of $\hat{\gamma}(\hat{A})_i$ and the asymptotic distribution given by Equation (11) for $i = 1, \dots, \hat{M}$. (c) Histogram of $\hat{\gamma}(\hat{A})_i$ for one particular choice of i alongside the asymptotic distribution given by Equation (11).

Repeating this 15 times for each combination of $\rho(\Phi)$ and T , we computed the mean NRMSE and mean ARI along with the corresponding standard error of the mean, respectively. Figure 1 (a) and (b) show that the NRMSE decreases both as $\rho(\Phi)$ increases and as T increases. Figure 1 (c) and (d) show that the ARI approaches 1 as the spectral radius approaches 1, meaning that the ground truth clusters are recovered in a high signal-to-noise regime.

4.2 Between block probability

Choosing simulation hyperparameters $N = 100$, $T = 1000$, $Q = 1$, $K = 10$, and setting $\tilde{\Phi}^{(1)}$ by sampling each entry from a Uniform(0,1) and normalising so that $\rho(\Phi^{(1)}) = 0.9$, we computed the percentage of incorrect entries of \hat{A} as a function of $p^{(out)}$. In particular, the percentage error was calculated as $100 \times \sum_{i,j=1}^N \mathbb{1}\{\hat{A}_{ij} \neq A_{ij}\} / N^2$. The percentage variable selection error of a LASSO estimator was computed for comparison, where the LASSO penalty hyperparameter was chosen using the Akaike Information Criterion (AIC) (Akaike, 1974). Figure 2(a) shows that the percentage error increases with $p^{(out)}$ and surpasses that of the LASSO estimator for $p^{(out)} > 0.05$. This is expected since the NIRVAR estimation procedure always constructs a graph with K cliques and cannot recover edges between blocks, which are deemed as noise.

4.3 Latent position recovery

We conduct a study in which we fix two ground truth latent positions $\theta_{B1} = (0.05, 0.95)'$ and $\theta_{B2} = (0.95, 0.05)'$ of the data generating SBM and compare the (rotated) NIRVAR embedded points $\hat{Y}^{(1)}$ to θ_{B1} and θ_{B2} . The hyperparameters used to generate the data were $N = 150$, $T = 2000$, $Q = 1$, $K = 2$, $z_1, \dots, z_{75} = 1$ and $z_{76}, \dots, z_{150} = 2$. The weights $\tilde{\Phi}$ were set to the constant $0.9/\rho(\Theta\Theta')$ so that the spectral radius of the expected value of Φ was 0.9. With $\mathbf{X}_t^{(1)} \sim \text{NIRVAR}(\Phi)$ for $t = 1, \dots, T$, the left singular vectors and singular values of $S^{(1)}$ were computed, and the singular values were scaled using $(\lambda_{\Phi})_i = \pm\sqrt{1 - 1/(\lambda_{\Gamma})_i}$ from Proposition 2.4.

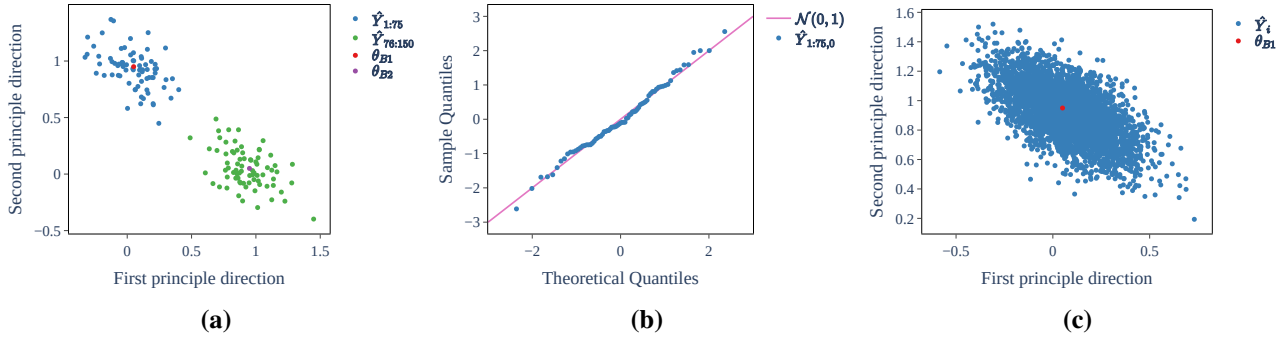


Figure 3: (a) NIRVAR embedded latent points (scaled and rotated) alongside the ground truth latent positions of the data generating SBM. (b) Q-Q plot comparing the sample distribution of the NIRVAR embedded points with a normal distribution. (c) The NIRVAR embedded latent position for $i = 21$ across 4000 replica samples.

Procrustes alignment (Schönemann, 1966) was then used to compare the rotated sample embedded points $\hat{Y}_{1:75}$ to θ_{B1} and $\hat{Y}_{76:150}$ to θ_{B2} . Figure 3(a) shows \hat{Y}_i coloured according to the block membership z_i for $i = 1, \dots, N$. Figure 3(b) shows a Q-Q plot comparing the (standardised) sample distribution $\hat{Y}_{1:75}$ with a standard normal distribution. The sample data is in good agreement with a normal distribution. We also conduct a further study in which we replicate the above procedure 4000 times and plot \hat{Y}_i for $i = 21$ against θ_{B1} across the 4000 replicas. Since $\rho(\Phi_k)$ (with $k \in \{1, \dots, 4000\}$ labelling the replica) has spectral radius less than 1 only in expectation, we only retain the first 4000 samples that have $\rho(\Phi_k) < 1$. Figure 3(c) shows that the large sample distribution of \hat{Y}_{21} is approximately normally distributed around θ_{B1} . Using the R package MVN (Korkmaz et al., 2014), we performed the Henze-Zirkler test of multivariate normality on the 4000 sample points yielding a test statistic of 0.56 and an observed p -value of 0.96 which supports the null hypothesis that the data is multivariate normally distributed.

4.4 Large sample distribution of the NIRVAR estimator

We simulate data with $N = 50$, $Q = 1$, $T = 5000$, $K = 5$, and set $\tilde{\Phi}^{(1)}$ by sampling each entry from a Uniform(0,1) and normalising so that $\rho(\tilde{\Phi}^{(1)}) = 0.9$. The probability of an edge forming within each block was set to $p^{(\text{in})} = 0.75$ and we set $p^{(\text{out})} = 0.2$. Creating 10,000 replica datasets, each having these hyperparameters, and estimating Φ for each replica provides an empirical distribution for $\sqrt{T}\hat{\gamma}(\hat{A})_i$. For each $i = 1, \dots, \hat{M}$, we performed a one-sample Kolmogorov-Smirnov (KS) test of whether the empirical distribution of $\sqrt{T}\hat{\gamma}(\hat{A})_i$ is normal with mean $\sqrt{T}C_\infty\gamma(A)$ and variance $\{R(\hat{A})'(\Gamma \otimes \Sigma^{-1})R(\hat{A})\}^{-1}$ as claimed by Proposition 3.2 to be its asymptotic distribution. The bias term, C_∞ is defined as

$$C_\infty := \text{plim}(C) = \{R(\hat{A})'(\Gamma \otimes \Sigma^{-1})R(\hat{A})\}^{-1}R(\hat{A})'(\Gamma \otimes \Sigma^{-1})R(A).$$

Figure 2(b) shows a box plot of the KS statistic for each $i = 1, \dots, \hat{M}$, whilst Figure 2(c) shows a histogram of the observed sample for one particular i plotted alongside the corresponding asymptotic normal curve. The low value of $\delta^{(\text{KS})}$ shown by the box plot in Figure 2(b) indicates that the large sample distribution of $\sqrt{T}\hat{\gamma}(\hat{A})_i$ is well captured by the asymptotic distribution of Proposition 3.2.

5 Applications

In this section, we apply the NIRVAR model to three different data sets: (1) the market excess returns of a panel of 648 financial assets, (2) the August 2022 vintage of the FRED-MD database (McCracken and Ng, 2016) which consists of 122 monthly macroeconomic variables, and (3) the number of daily bicycle rides leaving each of 774 Santander Cycles docking stations in central London between 07/03/2018 and 10/03/2020 (735 days). For each data set, we compare the predictive performance of NIRVAR against the Factor Augmented Regression Model (FARM) of Fan et al. (2023), the Factor-Adjusted Network Estimation and Forecasting for High-Dimensional

Time Series (FNETS) model of Barigozzi et al. (2023), and the Generalised Network Autoregressive Processes (GNAR) model of Knight et al. (2020). The details of each data set and the specific prediction task at hand are given below. For convenience, we briefly summarise below the three benchmark models from the literature.

1. **FARM** – In FARM, the stochastic process $X_{i,t}$ is modelled as

$$X_{i,t} = \mu_i + \lambda_i \sum_{\ell=1}^L \tau_\ell f_{t-\ell} + \sum_{\ell=1}^L \sum_{j=1}^N (\Delta_\ell)_{ij} \xi_{j,t-\ell} + \epsilon_{i,t},$$

where μ_i is the sample mean of series i , f_t is the leading factor at time t with λ_i the corresponding loading on this factor for series i , and $\xi_{j,t}$ is the residual value of series i after subtracting the contribution of the factor. The parameters τ_ℓ and Δ_ℓ are AR and VAR coefficients for the static factor model and idiosyncratic component, respectively. The factors and loadings are estimated using PCA, τ_ℓ is estimated via OLS, and $\Delta_{j,\ell}$ is estimated using LASSO, with a penalty parameter selected via BIC.

2. **FNETS** – In FNETS, the stochastic process \mathbf{X}_t is modelled as a sum of two latent components: a factor-driven common component χ_t , modelled as a generalised dynamic factor model (Forni et al., 2000), and an idiosyncratic component ξ_t , modelled as a VAR process. This results in the following model

$$\mathbf{X}_t = \chi_t + \xi_t, \quad \chi_t = \sum_{\ell=1}^{\infty} \Lambda_\ell \mathbf{f}_{t-\ell}, \quad \xi_t = \sum_{l=1}^L \Delta_l \xi_{t-l} + \Gamma^{1/2} \epsilon_t,$$

where $\mathbb{E}(\epsilon_t) = 0$ and $\text{cov}(\epsilon_t) = I_N$. Estimation of χ_t proceeds by dynamic PCA, whilst for ξ_t , Barigozzi et al. (2023) propose a ℓ_1 -regularised Yule-Walker estimator that requires second-order moments only.

3. **GNAR** – In GNAR, a simplified model for $X_{i,t}$ takes the form

$$X_{i,t} = \sum_{\ell=1}^L \left(\alpha_{i,\ell} X_{i,t-\ell} + \beta_\ell \sum_{j \in \mathcal{N}(i)} X_{j,t-\ell} \right) + \epsilon_{i,t}, \quad (12)$$

where $\mathcal{N}(i)$ denotes the set of vertices that are connected to vertex i of a known graph and $\mathbb{E}(\epsilon_{i,t}) = 0$ with $\text{var}(\epsilon_{i,t}) = \sigma_i^2$. The full GNAR model in Knight et al. (2020) extends Equation (12) allowing for a time varying known network, edge weights, multiple edge covariates, and stage-neighbours. A key difference between NIRVAR and GNAR is that GNAR assumes the network structure to be known, which is typically not the case in most real-world applications.

5.1 Financial Returns Prediction

The open-to-close (OPCL) and previous close-to-close (pvCLCL) price returns of 648 financial assets between 03/01/2000 and 31/12/2020 were derived from databases provided by the Center for Research in Security Prices, LLC, an affiliate of the University of Chicago Booth School of Business. Using the S&P 500 index as a proxy for the market, we construct the OPCL and pvCLCL market excess returns by subtracting the return of SPY, the exchange traded fund which tracks the S&P 500 index. The task is to predict the next day pvCLCL market excess returns. If the predicted next day pvCLCL market excess return of an asset has a positive (resp., negative) sign, then a long (resp., short) position in the asset is taken. We compare seven different models: NIRVAR using the covariance matrix embedding method with $Q = 1$ (pvCLCL returns only) and $Q = 2$ (pvCLCL and OPCL), labelled as NIRVAR C1 and NIRVAR C2, respectively; NIRVAR using the precision matrix embedding method with $Q = 1$ and $Q = 2$, labelled as NIRVAR P1 and NIRVAR P2, respectively; FARM with $L = 1$; FNETS with $L = 1$; GNAR with $L = 1$ and $j \in \mathcal{N}(i)$ iff asset i and asset j share the same Standard Industrial Classification (SIC) division. The SIC assigns a four-digit code to businesses according to their industry; the codes are available at <https://siccode.com/>. Every business is in one of the following 10 sector divisions: (i) Agriculture, Forestry, and Fishing, (ii) Mining, (iii) Construction, (iv) Manufacturing, (v) Transportation and Public Utilities, (vi) Wholesale Trade, (vii) Retail Trade, (viii) Finance, Insurance, and Real Estate, (ix) Services, and (x) Public Administration.

We backtest each model using a rolling window between 01/01/2004 and 31/12/2020 with a look-back window of four years, and we evaluate the performance via a number of commonly used metrics in the financial literature (see, for example, [Avellaneda and Lee, 2010](#)). Each day, we compute a measure of profit and loss (PnL), defined on day t as

$$\text{PnL}_t = \sum_{i=1}^N \text{sign} \left(\hat{s}_i^{(t)} \right) \times s_i^{(t)},$$

where $\hat{s}_i^{(t)}$ is the predicted return of asset i on day t , and $s_i^{(t)}$ is the realized return of asset i on day t . Note that we assign an equal portfolio weighting to each asset in our definition of PnL_t ; an alternative approach would be to consider value-weighted portfolio construction methods, that account for the liquidity of each asset. Doing this every day for T backtesting days, we obtain the time series $\{\text{PnL}_t\}_{t=1, \dots, T} := \text{PnL}$. The cumulative PnL for each model is shown in Figure 4(a). The NIRVAR models outperform FNETS, GNAR and FARM in terms of cumulative PnL, and NIRVAR P1 attains the highest cumulative PnL overall. We plot the cumulative PnL of NIRVAR P1 for different levels of transaction costs in Figure 4(b), where a flat transaction cost (given in basis points, denoted *bpts*, with 1% = 100bpts) is applied every time we flip our position in a given asset from long (short) to short (long). From Figure 4(b) we conclude that, even with a transaction cost of 4bpts, NIRVAR is profitable, especially during the global financial crisis and the COVID-19 pandemic which were periods of high market volatility. Table 1 compares each model across 8 statistics often used in the literature on financial returns prediction (see, for example [Gu et al., 2020](#)). One of the most common metrics used in the financial industry is the annualised Sharpe ratio, defined as

$$\text{SR} = \frac{\text{mean}(\text{PnL})}{\text{stdev}(\text{PnL})} \times \sqrt{252},$$

where the scaling is due to the fact that there are 252 trading days within a year. Definitions of the other statistics used are provided in Appendix B.1 of the online supplementary material.

Figure 5(a) compares the NIRVAR estimated clusters with the 10 SIC sectors on one particular backtesting day. Figure 5(b) shows the corresponding ARI for every backtesting day. The ARI never breaches 0.17, from which we conclude that the NIRVAR estimated clusters do not recover the SIC groupings, which, by no means, should be treated as ground truth. The bar chart does suggest, however, that NIRVAR tends to separate Finance, Insurance, and Real Estate companies from the other SIC groups. Figure 5(c) provides the ARI between the NIRVAR estimated clusters at time t and the NIRVAR estimated clusters at time s , where t and s run over every pair of backtesting days. There are two distinct blocks along the diagonal of this heatmap, the first one between 2004-2008 and the second one between 2008-2013, indicating that the NIRVAR estimated clusters underwent a shift after the global financial crisis.

Table 2 provides the Sharpe ratio of each model on five equally-spaced intervals of the backtesting period. NIRVAR performs particularly well around the time of the global financial crisis. We also note that NIRVAR P2 and NIRVAR C2 are the best performing models in the fourth sub-period considered, suggesting that the extra feature is beneficial in this period.

5.2 Forecasting US Industrial Production

FRED-MD is a publicly accessible database of monthly observations of macroeconomic variables. It is updated in real-time and is available from Michael McCracken’s webpage¹. Also available from this webpage is an R package to transform the raw data into a stationary series, which we use. The details of the transformations used can be found at [McCracken and Ng \(2016\)](#). To allow direct comparison with [Fan et al. \(2023\)](#), we choose the August 2022 vintage of the FRED-MD database which extends from January 1960 until December 2019 (719 observations). Only variables with no missing values (122 variables) are used.

¹<https://research.stlouisfed.org/econ/mccracken/fred-databases/>

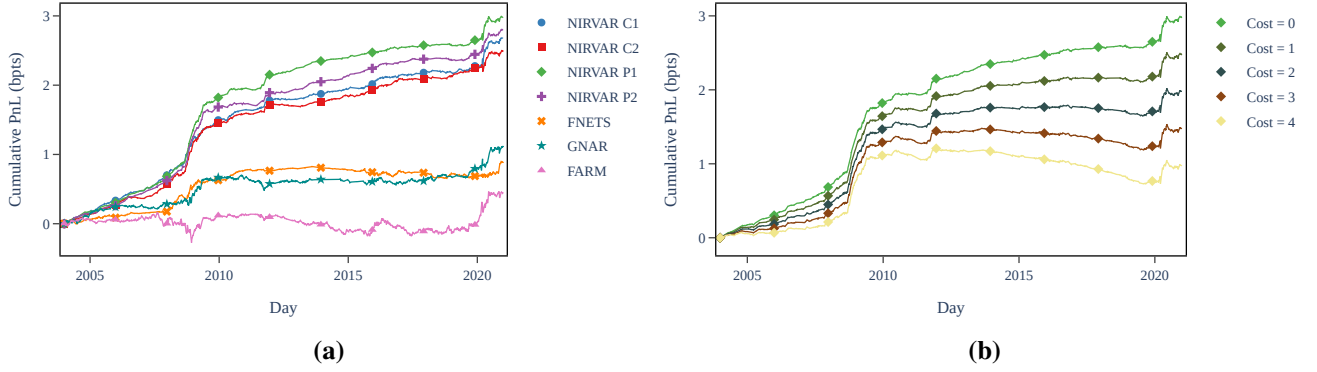


Figure 4: (a) The cumulative PnL in bpts for the 7 models over the backtesting period with zero transaction costs. (b) The cumulative PnL of NIRVAR P1 for different levels of transaction costs.

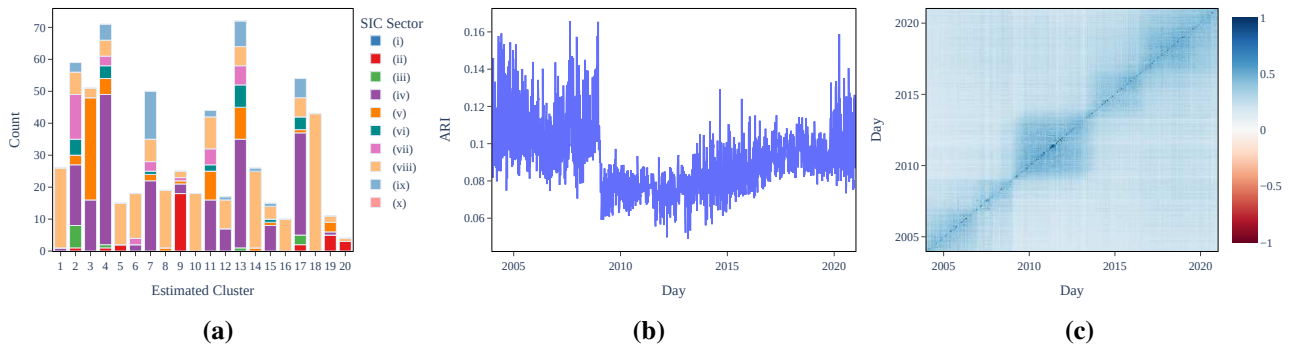


Figure 5: (a) Comparison of the NIRVAR estimated clusters with the SIC groups on 31/12/2020. (b) The ARI between the NIRVAR estimated clusters and the SIC groups on each backtesting day. (c) The ARI between NIRVAR estimated clusters on different days within the backtesting period.

Table 1: Statistics on the financial returns predictive performance of each model over the backtesting period. Note that “N” is an abbreviation of NIRVAR. The best performing model is shown in bold, whilst the second best performing model is underlined.

	N C1	N C2	N P1	N P2	FARM	FNETS	GNAR
Sharpe Ratio	2.50	2.34	2.82	<u>2.69</u>	0.22	0.78	0.70
Sortino Ratio	4.57	4.18	4.80	<u>4.63</u>	0.36	1.39	1.13
Maximum Drawdown (%)	111	170	<u>61</u>	48	531	107	257
Hit Ratio (%)	50.6	50.6	50.7	50.7	48.7	50.2	41.5
Long Ratio (%)	<u>50.1</u>	49.8	<u>50.1</u>	50.0	49.0	<u>50.1</u>	40.7
Mean RMSE	0.018	0.019	0.018	0.019	0.018	0.018	0.018
Mean Daily PnL (bpts)	2.68	2.49	3.00	<u>2.79</u>	0.44	0.89	1.10
Mean Absolute Error	0.012	0.013	0.012	0.013	0.012	0.012	0.012

The prediction task is one-step ahead forecasts of the first-order difference of the logarithm of the monthly industrial production (IP) index. We backtest each model from January 2000 until December 2019 using a rolling window framework with a lookback window of 480 observations. We choose the covariance matrix embedding method of NIRVAR. Following Fan et al. (2023), we set $L = 24$ for FARM. For FNETS and GNAR we set $L = 1$. The FRED-MD variables are divided into eight groups: (i) output and income; (ii) labour market; (iii) housing; (iv) consumption, orders, and inventories; (v) money and credit; (vi) interest and exchange rates; (vii) prices; and

Table 2: Annualised Sharpe ratios over five equally periods from 01/01/2004 - 31/12/2020. The best performing model is shown in bold, whilst the second best performing model is underlined.

	N C1	N C2	N P1	N P2	FARM	FNETS	GNAR
01/01/2004 - 31/05/2007	4.44	3.09	5.14	<u>4.49</u>	0.56	1.17	1.11
01/06/2007 - 21/10/2010	3.87	4.28	5.08	<u>4.60</u>	0.02	2.05	1.14
22/10/2010 - 19/03/2014	1.91	1.41	3.10	<u>2.36</u>	-0.56	0.46	-0.22
20/03/2014 - 09/08/2017	1.78	<u>2.04</u>	1.41	2.38	-0.37	-0.28	-0.06
10/08/2017 - 31/12/2020	1.70	1.34	<u>1.37</u>	<u>1.37</u>	1.10	0.45	1.07

Table 3: Overall MSE and regime statistics of each model for the task of forecasting US IP. The best performing model is shown in bold, whilst the second best performing model is underlined.

	NIRVAR	FARM	FNETS	GNAR
Overall MSE	0.0087	<u>0.0089</u>	0.0096	0.0101
MSE: under-estimated	0.0070	<u>0.0076</u>	0.0092	0.0087
MSE: over-estimated	0.0017	<u>0.0013</u>	0.0003	0.0015
MSE: non-extreme	0.0042	0.0042	0.0039	<u>0.0041</u>
MSE: extreme	0.0045	<u>0.0047</u>	0.0057	0.0060

(viii) stock market. The network we choose for GNAR is defined by $j \in \mathcal{N}(i)$ if and only if i, j are in the same FRED-MD group.

Figure 6 shows the realised difference of the logarithm of IP against the corresponding prediction of each model. Figure 6(a) and Figure 6(d) show that both NIRVAR and FARM are more reactive to extreme values than FNETS and GNAR, shown in Figure 6(b) and Figure 6(c), respectively. Table 3 reports the overall MSE, the sum of the MSE at points for which the model over (under)-estimated the realised value, and the sum of the MSE in extreme and non-extreme regimes where a realised value is defined to be extreme if its magnitude is above the 90-th quantile. In Figure 7(a), the ratio of cumulative MSEs between NIRVAR and each of FNETS, GNAR, and FARM is plotted. In particular, letting $\Delta_t^{(m)}$ be the ratio for model $m \in \{\text{FNETS, GNAR, FARM}\}$ at time $t \in \{1, \dots, T\}$, we have

$$\Delta_t^{(m)} := \frac{\sum_{s=1}^t \text{MSE}_s^{(\text{NIRVAR})}}{\sum_{s=1}^t \text{MSE}_s^{(m)}}.$$

A value of $\Delta_t^{(m)}$ that is less than 1 indicates that NIRVAR is outperforming model m in terms of cumulative MSE. $\Delta_t^{(m)}$ is always below 1 for GNAR and FNETS, and for FARM it is below 1 the majority of the time. Figure 7(b) compares the NIRVAR estimated clusters with the eight FRED groups on one particular backtesting day. Overall, the NIRVAR clusters do not match the FRED-MD groups closely, although NIRVAR clusters 2,4,10,11, and 12 consist almost entirely of a single FRED-MD group. This low-to-medium level matching between NIRVAR clusters and FRED-MD groups is captured by Figure 7(c), which shows that the ARI for every backtesting day lies in the range [0.24,0.36]. We conclude that the human defined FRED-MD groups are not necessarily the most useful course grained description if one is interested in co-movements between time series of the 122 macroeconomic variables.

5.3 Forecasting Santander bicycle rides

The log daily number of bicycle rides from 774 Santander stations in London from 07/03/2018 until 10/03/2020 ($T = 735$) were obtained using data from <https://cycling.data.tfl.gov.uk/>. First differences were then taken in order to obtain stationary time series. NIRVAR, FARM, FNETS and GNAR were used to predict the next

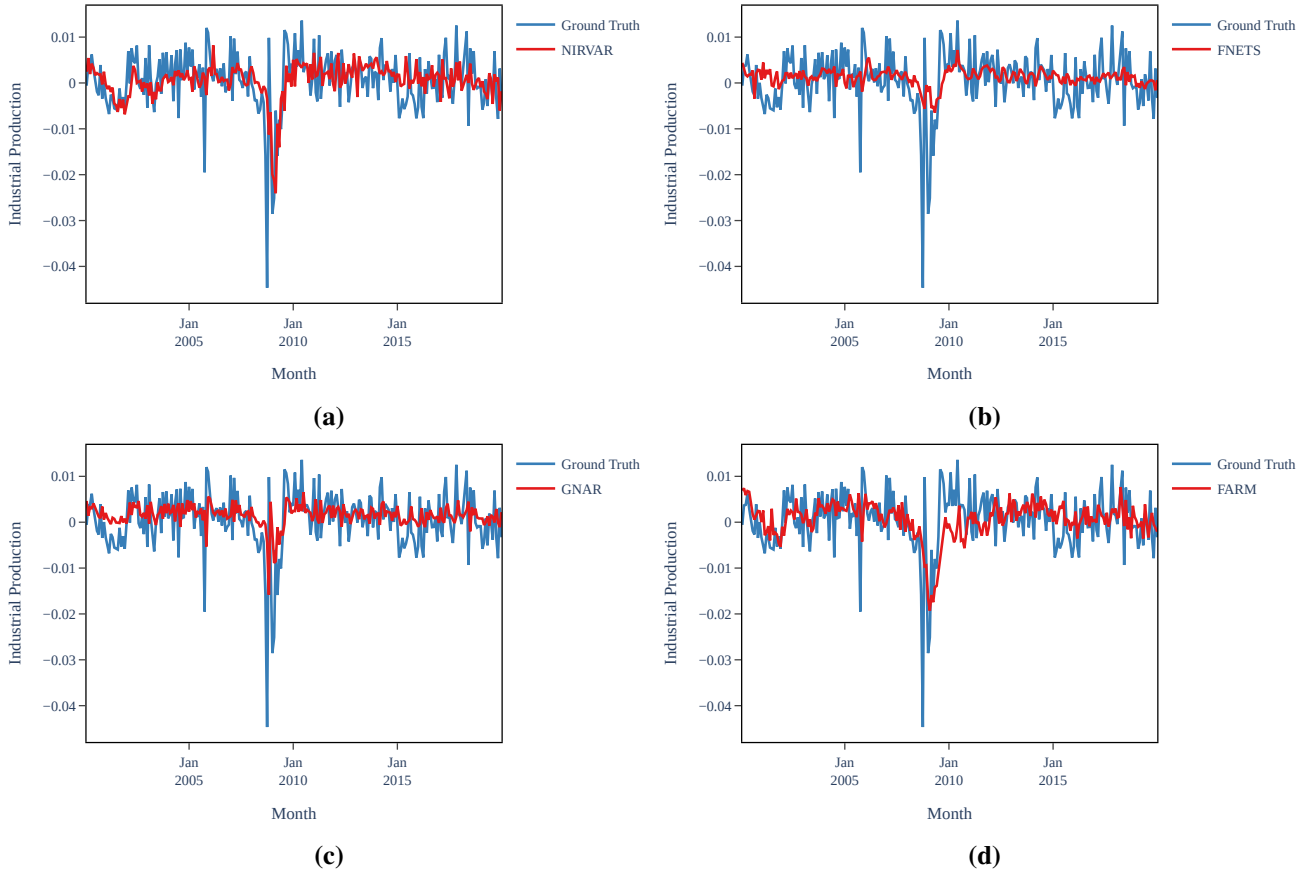


Figure 6: Predicted (log-differenced) IP against the realised (log-differenced) IP for each model.

day log number of bicycle rides using a rolling window backtesting framework from 09/02/2020 until 10/03/2020 (30 days). Since $N > T$ in this example, the covariance matrix is not invertible and therefore the NIRVAR precision matrix embedding method is not feasible here. FARM, FNETS and GNAR are modelled using a lag of $L = 1$. The network we choose for GNAR is defined by $j \in \mathcal{N}(i)$ if and only if the Euclidean distance between station j and station i is less than 3 kilometers. The one-step-ahead MSE, $\|\hat{\mathbf{X}}_t - \mathbf{X}_t\|_2^2$, is shown for each model in Table 4. NIRVAR achieves the lowest overall MSE.

There were $K = 7$ clusters estimated by NIRVAR. Figure 8(a) shows the geographic locations of the stations in NIRVAR clusters 3 and 5. Cluster 5 is concentrated around central London whereas the stations in cluster 3 are located further from the center near parks and more residential areas. In contrast to the human defined epsilon ball construction of the GNAR network, the NIRVAR clusters do not always lie within some ball of a given radius. Figure 8(b) shows the mean number of bicycle rides across each of the 7 NIRVAR clusters for every day of the week. The clusters are differentiated by their mean number of bicycle rides as well as by the change in the number of bicycle rides on weekdays compared with weekends. For example, stations in clusters 2 and 5, which are located mainly in central London, have high usage during the week and lower usage during the weekend. This likely corresponds to usage by professionals commuting to work. In contrast, the usage of bicycles from stations in cluster 3 increases at the weekends. This may correspond to usage by tourists and residential home owners that live outside of central London.

To understand the flow of bicycle rides between NIRVAR clusters, we computed a $K \times K$ matrix F , where F_{ij} is the number of bicycle rides that start from any station in cluster i and end in any station in cluster j . A matrix \tilde{F} with elements

$$\tilde{F}_{ij} = \frac{F_{ij} - F_{ji}}{F_{ij} + F_{ji}},$$

provides a normalised measure of the imbalance in the flow of bicycle rides between NIRVAR clusters. Figure

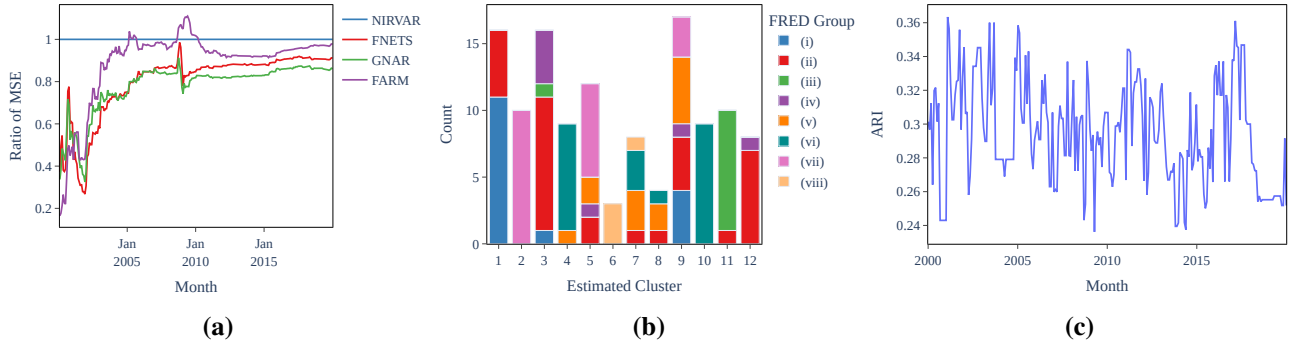


Figure 7: (a) Ratio, $\Delta_t^{(m)}$, of the cumulative MSE of NIRVAR divided by the cumulative MSE of FNETS/GNAR/FARM. (b) Comparison of the NIRVAR estimated clusters with the FRED groups for January 2000. (c) The ARI between the NIRVAR estimated clusters and the FRED groups on month between January 2000 - December 2019.

Table 4: Overall MSE of each model for the task of predicting the log number of bicycle rides from each Santander station. The best performing model is shown in bold, whilst the second best performing model is underlined.

	NIRVAR	FARM	FNETS	GNAR
Overall MSE	0.364	<u>0.370</u>	0.388	0.374

8(c) shows \tilde{F}_{ij} . Rows 2 and 5 of \tilde{F} are negative (red) which corresponds to a net inflow into NIRVAR clusters 2 and 5, whose stations are located mainly in central London.

6 Discussion

In this work, we introduce NIRVAR, a framework for modelling a panel of multivariate time series as a network VAR process when the underlying network is unobserved. The NIRVAR estimation method differs from existing network VAR methods by proposing a network representation of the panel components prior to estimation of the VAR model parameters. This circumvents the need to specify tuning or thresholding hyperparameters when constructing the network, and it avoids estimation of the full, dense VAR parameter matrix. NIRVAR can accommodate multiple edge types in the form of a multiplex graph and has better predictive performance compared with other network time series methods on three applications in finance, macroeconomics and transportation. Due to the regularisation induced by the network, NIRVAR is computationally much faster than a VAR. For example, back-testing NIRVAR on the Santander experiment in Section 5.3 for a single forecast took approximately 10 seconds compared with approximately 70 seconds for a VAR².

A drawback of the estimation method is that it will be biased whenever there are edges between blocks of the data generating SBM. Therefore, it is only suitable for assortative graphs. One possible solution to this is to consider a mixed membership SBM (Airoldi et al., 2008) in which each graph vertex can be associated with multiple clusters. We leave this for future research. The NIRVAR model assumes the observed random graph does not change over time. Extending the model to incorporate a time varying adjacency matrix could add flexibility and improve both the cluster assignment and the predictive performance of the framework.

It would be a natural extension to incorporate a factor model into the NIRVAR framework. The advantage of this would be to isolate the idiosyncratic interactions that are due to network effects from the co-movements that are due to common factors. For example, in the financial application, we removed the market factor prior to NIRVAR estimation. It would be straightforward to include more factors, such as those of the Fama-French five factor model (Fama and French, 2015), before applying NIRVAR estimation. Incorporating a factor model would also likely improve the forecasting performance of NIRVAR on the FRED-MD dataset. McCracken and Ng (2016)

²Both experiments were run using a single Intel Core i5-1145G7 CPU.

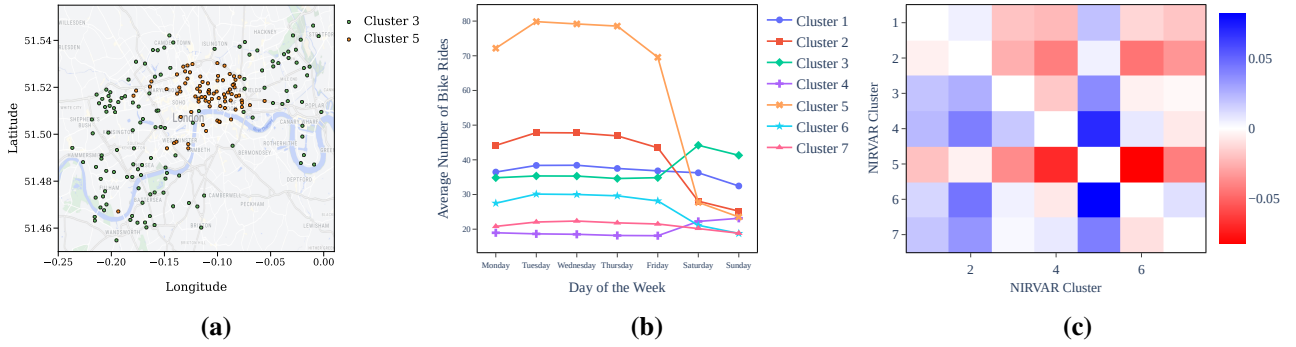


Figure 8: (a) NIRVAR clusters 3 and 5 obtained on the Santander bicycle data set. (b) The mean number of bicycle rides across each of the $K = 7$ NIRVAR clusters for every day of the week. (c) The matrix \hat{F} which gives a measure of the imbalance of flow between each pair of NIRVAR clusters. If \hat{F}_{ij} is blue then there is a net flow from cluster i into cluster j , whereas if \hat{F}_{ij} is red then the flow is from cluster j to cluster i .

find eight factors in the sample they consider; removing these factors could give prominence to network effects, thus improving NIRVAR estimation and prediction.

Acknowledgements

Brendan Martin acknowledges funding from the Engineering and Physical Sciences Research Council (EPSRC), grant number EP/S023151/1. Francesco Sanna Passino acknowledges funding from the EPSRC, grant number EP/Y002113/1.

Data availability

All data and *Python* code are available in the GitHub repository [bmartin9/NIRVAR](https://github.com/bmartin9/NIRVAR).

References

- Ahelegbey, D. F., Billio, M., and Casarin, R. (2016) Bayesian graphical models for structural vector autoregressive processes. *Journal of Applied Econometrics*, **31**, 357–386.
- Airoldi, E. M., Blei, D., Fienberg, S., and Xing, E. (2008) Mixed membership stochastic blockmodels. *Advances in Neural Information Processing Systems*, **21**.
- Akaike, H. (1974) A new look at the statistical model identification. *IEEE Transactions on Automatic Control*, **19**, 716–723.
- Athreya, A., Fishkind, D. E., Tang, M., et al. (2017) Statistical inference on random dot product graphs: a survey. *The Journal of Machine Learning Research*, **18**, 8393–8484.
- Athreya, A., Tang, M., Park, Y., and Priebe, C. E. (2021) On estimation and inference in latent structure random graphs. *Statistical Science*, **36**, 68–88.
- Avellaneda, M. and Lee, J.-H. (2010) Statistical arbitrage in the us equities market. *Quantitative Finance*, **10**, 761–782.
- Bai, J. (2003) Inferential theory for factor models of large dimensions. *Econometrica*, **71**, 135–171.
- Bai, Z. and Silverstein, J. W. (2010) *Spectral analysis of large dimensional random matrices*, vol. 20. Springer.

- Barigozzi, M., Cavaliere, G., and Moramarco, G. (2022) Factor network autoregressions. *arXiv preprint arXiv:2208.02925*.
- Barigozzi, M., Cho, H., and Owens, D. (2023) FNETS: Factor-adjusted network estimation and forecasting for high-dimensional time series. *Journal of Business & Economic Statistics*, 1–13.
- Cayton, L. et al. (2008) *Algorithms for manifold learning*. eScholarship, University of California.
- Chang, J., He, J., Yang, L., and Yao, Q. (2023) Modelling matrix time series via a tensor cp-decomposition. *Journal of the Royal Statistical Society (Series B)*, **85**, 127–148.
- Chen, E. Y., Fan, J., and Zhu, X. (2023) Community network auto-regression for high-dimensional time series. *Journal of Econometrics*, **235**, 1239–1256.
- Dahlhaus, R. (2000) Graphical interaction models for multivariate time series. *Metrika*, **51**, 157–172.
- De Domenico, M., Solé-Ribalta, A., Cozzo, E., et al. (2013) Mathematical formulation of multilayer networks. *Physical Review X*, **3**, 041022.
- Dempster, A. P., Laird, N. M., and Rubin, D. B. (1977) Maximum likelihood from incomplete data via the EM algorithm. *Journal of the Royal Statistical Society (Series B)*, **39**, 1–22.
- Donoho, D., Gavish, M., and Romanov, E. (2023) Screenot: Exact mse-optimal singular value thresholding in correlated noise. *The Annals of Statistics*, **51**, 122–148.
- Efron, B., Hastie, T., Johnstone, I., and Tibshirani, R. (2004) Least angle regression. *The Annals of Statistics*, **32**, 407–451.
- Eichler, M. (2007) Granger causality and path diagrams for multivariate time series. *Journal of Econometrics*, **137**, 334–353.
- Fama, E. F. and French, K. R. (2015) A five-factor asset pricing model. *Journal of Financial Economics*, **116**, 1–22.
- Fan, J. and Li, R. (2001) Variable selection via nonconcave penalized likelihood and its oracle properties. *Journal of the American Statistical Association*, **96**, 1348–1360.
- Fan, J., Liao, Y., and Mincheva, M. (2013) Large covariance estimation by thresholding principal orthogonal complements. *Journal of the Royal Statistical Society (Series B)*, **75**, 603–680.
- Fan, J., Masini, R. P., and Medeiros, M. C. (2023) Bridging factor and sparse models. *The Annals of Statistics*, **51**, 1692–1717.
- Ferguson, T. S. (2017) *A course in large sample theory*. Routledge.
- Fletcher, R. (2000) *Practical methods of optimization*. John Wiley & Sons.
- Forni, M., Hallin, M., Lippi, M., and Reichlin, L. (2000) The generalized dynamic-factor model: Identification and estimation. *Review of Economics and Statistics*, **82**, 540–554.
- Gallagher, I., Jones, A., Bertiger, A., Priebe, C. E., and Rubin-Delanchy, P. (2023) Spectral embedding of weighted graphs. *Journal of the American Statistical Association*, 1–10.
- Gallagher, I., Jones, A., and Rubin-Delanchy, P. (2021) Spectral embedding for dynamic networks with stability guarantees. *Advances in Neural Information Processing Systems*, **34**, 10158–10170.
- Gu, S., Kelly, B., and Xiu, D. (2020) Empirical asset pricing via machine learning. *The Review of Financial Studies*, **33**, 2223–2273.

- Guðmundsson, G. S. and Brownlees, C. (2021) Detecting groups in large vector autoregressions. *Journal of Econometrics*, **225**, 2–26.
- Holland, P. W., Laskey, K. B., and Leinhardt, S. (1983) Stochastic blockmodels: First steps. *Social networks*, **5**, 109–137.
- Hubert, L. and Arabie, P. (1985) Comparing partitions. *Journal of Classification*, **2**, 193–218.
- Johnstone, I. M. (2001) On the distribution of the largest eigenvalue in principal components analysis. *The Annals of statistics*, **29**, 295–327.
- Jones, A. and Rubin-Delanchy, P. (2020) The multilayer random dot product graph. *arXiv preprint arXiv:2007.10455*.
- Knight, M., Leeming, K., Nason, G., and Nunes, M. (2020) Generalized network autoregressive processes and the GNAR package. *Journal of Statistical Software*, **96**, 1–36.
- Knight, M. I., Nunes, M., and Nason, G. (2016) Modelling, detrending and decorrelation of network time series. *arXiv preprint arXiv:1603.03221*.
- Korkmaz, S., Gökşülük, D., and Zararsiz, G. (2014) MVN: An R package for assessing multivariate normality. *R Journal*, **6**.
- Laloux, L., Cizeau, P., Potters, M., and Bouchaud, J.-P. (2000) Random matrix theory and financial correlations. *International Journal of Theoretical and Applied Finance*, **3**, 391–397.
- Lancichinetti, A. and Fortunato, S. (2009) Community detection algorithms: a comparative analysis. *Physical review E*, **80**, 056117.
- Lee, C. and Wilkinson, D. J. (2019) A review of stochastic block models and extensions for graph clustering. *Applied Network Science*, **4**, 1–50.
- Lütkepohl, H. (2005) *New introduction to multiple time series analysis*. Springer Science & Business Media.
- Marčenko, V. A. and Pastur, L. A. (1967) Distribution of eigenvalues for some sets of random matrices. *Matematicheskii Sbornik*, **114**, 507–536.
- McCracken, M. W. and Ng, S. (2016) FRED-MD: A monthly database for macroeconomic research. *Journal of Business & Economic Statistics*, **34**, 574–589.
- Rubin-Delanchy, P., Cape, J., Tang, M., and Priebe, C. E. (2022) A statistical interpretation of spectral embedding: The generalised random dot product graph. *Journal of the Royal Statistical Society (Series B)*, **84**, 1446–1473.
- Schönemann, P. H. (1966) A generalized solution of the orthogonal procrustes problem. *Psychometrika*, **31**, 1–10.
- Shojaie, A. and Fox, E. B. (2022) Granger causality: A review and recent advances. *Annual Review of Statistics and Its Application*, **9**, 289–319.
- Smith, R. (1968) Matrix equation $xa+bx=c$. *SIAM Journal on Applied Mathematics*, **16**, 198–201.
- Sortino, F. A. and Price, L. N. (1994) Performance measurement in a downside risk framework. *the Journal of Investing*, **3**, 59–64.
- Stock, J. H. and Watson, M. W. (2002) Forecasting using principal components from a large number of predictors. *Journal of the American Statistical Association*, **97**, 1167–1179.
- Tibshirani, R. (1996) Regression shrinkage and selection via the lasso. *Journal of the Royal Statistical Society (Series B)*, **58**, 267–288.

- Whiteley, N., Gray, A., and Rubin-Delanchy, P. (2022) Statistical exploration of the manifold hypothesis. *arXiv preprint arXiv:2208.11665*.
- Wu, Z., Pan, S., Long, G., et al. (2020) Connecting the dots: Multivariate time series forecasting with graph neural networks. In *Proceedings of the 26th ACM SIGKDD International Conference on Knowledge Discovery & Data Mining*, 753–763.
- Young, N. (1981) The rate of convergence of a matrix power series. *Linear Algebra and its Applications*, **35**, 261–278.
- Zhang, M. and Chen, Y. (2018) Link prediction based on graph neural networks. *Advances in neural information processing systems*, **31**.
- Zhu, M. and Ghodsi, A. (2006) Automatic dimensionality selection from the scree plot via the use of profile likelihood. *Computational Statistics & Data Analysis*, **51**, 918–930.
- Zhu, X., Huang, D., Pan, R., and Wang, H. (2020) Multivariate spatial autoregressive model for large scale social networks. *Journal of Econometrics*, **215**, 591–606.
- Zhu, X., Pan, R., Li, G., Liu, Y., and Wang, H. (2017) Network vector autoregression. *The Annals of Statistics*, **45**, 1096 – 1123.

A Theory

A.1 Proof of Proposition 2.4

Proof. We prove that the covariance matrix $\Gamma = \mathbb{E}(\mathbf{X}_t \mathbf{X}_t')$ can be written in terms of U_Φ . From Lütkepohl (2005), we have that $\Gamma - \Phi \Gamma \Phi' = \Sigma$. This is an example of a Lyapunov matrix equation and its formal solution is given by (Young, 1981):

$$\Gamma = \sum_{k=0}^{\infty} (\Phi)^k \Sigma (\Phi')^k,$$

which converges when $\rho(\Phi) < 1$ (Smith, 1968). Since we assume a stationary NIRVAR process, then indeed $\rho(\Phi) < 1$ and the series converges. With $\Sigma = \sigma^2 I_N$ we have

$$\Gamma = \sigma^2 \sum_{k=0}^{\infty} (\Phi)^k (\Phi')^k = \sigma^2 (I_N - \Phi \Phi')^{-1}. \quad (13)$$

Recalling the eigendecomposition

$$\Phi = U_\Phi \Lambda_\Phi U_\Phi' + U_{\Phi,\perp} \Lambda_{\Phi,\perp} U_{\Phi,\perp}', \quad (14)$$

we can substitute Equation (14) into Equation (13),

$$\begin{aligned} \Gamma &= \sigma^2 \sum_{k=0}^{\infty} (U_\Phi \Lambda_\Phi U_\Phi' + U_{\Phi,\perp} \Lambda_{\Phi,\perp} U_{\Phi,\perp}')^k [(U_\Phi \Lambda_\Phi U_\Phi' + U_{\Phi,\perp} \Lambda_{\Phi,\perp} U_{\Phi,\perp}')^k] \\ &= \sigma^2 \left(I_N - U_\Phi U_\Phi' - U_{\Phi,\perp} U_{\Phi,\perp}' + U_\Phi \sum_{k=0}^{\infty} \Lambda_\Phi^{2k} U_\Phi' + U_{\Phi,\perp} \sum_{k=0}^{\infty} \Lambda_{\Phi,\perp}^{2k} U_{\Phi,\perp}' \right) \\ &= \sigma^2 (I_N - U_\Phi U_\Phi' - U_{\Phi,\perp} U_{\Phi,\perp}' + U_\Phi \Lambda_\Gamma U_\Phi' + U_{\Phi,\perp} \Lambda_{\Gamma,\perp} U_{\Phi,\perp}'), \end{aligned}$$

where Λ_Γ is a diagonal matrix whose diagonal entries are $(\lambda_\Gamma)_i = 1/(1 - (\lambda_\Phi)_i^2)$ with $(\lambda_\Phi)_i$ being the i -th diagonal entry of Λ_Φ . Note that $(\lambda_\Phi)_i \in (-1, 1)$ since we assume $\rho(\Phi) < 1$. Now $I_N - U_\Phi U_\Phi'$ and $U_{\Phi, \perp} U_{\Phi, \perp}'$ are both projection operators onto the column space of $U_{\Phi, \perp}$. Therefore, the rank d eigendecomposition of Γ is $\Gamma = U_\Phi \Lambda_\Gamma U_\Phi'$. \square

A.2 Proof of Proposition 3.1

Proof. We have that $\text{colsp}\{R(A)\} \subseteq \text{colsp}\{R(\hat{A})\} \iff R(\hat{A})\gamma(\hat{A}) = R(A)\gamma(A) = \beta$. This is true if and only if

$$\begin{aligned} \mathbb{E}\{\hat{\beta}(\hat{A})|\hat{A}\} &= \mathbb{E}(R(\hat{A})\hat{\gamma}(\hat{A})|\hat{A}) = R(\hat{A})\mathbb{E}[\{R(\hat{A})'(ZZ' \otimes \Sigma^{-1})R(\hat{A})\}^{-1}R(\hat{A})'(ZZ' \otimes \Sigma^{-1})R(A)\gamma(A)|\hat{A}] \\ &= R(\hat{A})\mathbb{E}[\{R(\hat{A})'(ZZ' \otimes \Sigma^{-1})R(\hat{A})\}^{-1}R(\hat{A})'(ZZ' \otimes \Sigma^{-1})R(\hat{A})\gamma(\hat{A})|\hat{A}] = R(\hat{A})\gamma(\hat{A}) = \beta. \quad \square \end{aligned}$$

A.3 Proof of Proposition 3.2

Proof. The NIRVAR estimator,

$$\begin{aligned} \hat{\gamma}(\hat{A}) &= \{R(\hat{A})'(ZZ' \otimes \Sigma^{-1})R(\hat{A})\}^{-1}R(\hat{A})'(ZZ' \otimes \Sigma^{-1})R(A)\gamma(A) \\ &\quad + \{R(\hat{A})'(ZZ' \otimes \Sigma^{-1})R(\hat{A})\}^{-1}R(\hat{A})'(I_{NQ} \otimes \Sigma^{-1})\text{vec}(U^{(q)}Z'). \end{aligned}$$

can be written as

$$\sqrt{T} \left\{ \hat{\gamma}(\hat{A}) - C\gamma(A) \right\} = \left\{ R(\hat{A})' \left(\frac{ZZ'}{T} \otimes \Sigma^{-1} \right) R(\hat{A}) \right\}^{-1} R(\hat{A})'(I_{NQ} \otimes \Sigma^{-1}) \frac{1}{\sqrt{T}} \text{vec}(U^{(q)}Z'). \quad (15)$$

By Lemma 3.1 of Lütkepohl (2005), Γ exists and is nonsingular. Also by Lemma 3.1 of Lütkepohl (2005),

$$\frac{1}{\sqrt{T}} \text{vec}(U^{(q)}Z') \xrightarrow{d} \mathcal{N}(0, \Gamma \otimes \Sigma). \quad (16)$$

By Equation (15),

$$\begin{aligned} \text{plim} \left\{ \hat{\gamma}(\hat{A}) - C\gamma(A) \right\} &= \text{plim} \left[\left\{ R(\hat{A})' \left(\frac{ZZ'}{T} \otimes \Sigma^{-1} \right) R(\hat{A}) \right\}^{-1} R(\hat{A})'(I_{NQ} \otimes \Sigma^{-1}) \text{vec} \left(\frac{U^{(q)}Z'}{T} \right) \right] \\ &= \text{plim} \left[\left\{ R(\hat{A})' \left(\frac{ZZ'}{T} \otimes \Sigma^{-1} \right) R(\hat{A}) \right\}^{-1} R(\hat{A})'(I_{NQ} \otimes \Sigma^{-1}) \right] \text{plim} \left\{ \text{vec} \left(\frac{U^{(q)}Z'}{T} \right) \right\}, \end{aligned}$$

where the second line follows from Slutsky's Theorem (see, for example Ferguson, 2017, Theorem 6(c)) and the continuous mapping theorem. But Equation (16) implies that

$$\text{plim} \left\{ \text{vec} \left(\frac{U^{(q)}Z'}{T} \right) \right\} = 0.$$

Thus $\text{plim}\{\hat{\gamma}(\hat{A}) - C\gamma(A)\} = 0$ (weak consistency). For convenience, we define

$$\hat{G} := \left\{ R(\hat{A})' \left(\frac{ZZ'}{T} \otimes \Sigma^{-1} \right) R(\hat{A}) \right\}^{-1} R(\hat{A})'(I_{NQ} \otimes \Sigma^{-1}).$$

Then

$$G := \text{plim}(\hat{G}) = \left\{ R(\hat{A})' (\Gamma \otimes \Sigma^{-1}) R(\hat{A}) \right\}^{-1} R(\hat{A})'(I_{NQ} \otimes \Sigma^{-1}).$$

By Proposition C.15(1) of Lütkepohl (2005), Equation (16) implies that

$$\hat{G} \frac{1}{\sqrt{T}} \text{vec}(U^{(q)} Z') \xrightarrow{d} \mathcal{N}(0, G(\Gamma \otimes \Sigma)G').$$

Thus, $\sqrt{T}\{\hat{\gamma}(\hat{A}) - C\gamma(A)\}$ is asymptotically normal with asymptotic variance

$$\begin{aligned} G(\Gamma \otimes \Sigma)G' &= \\ & \left[\left\{ R(\hat{A})' (\Gamma \otimes \Sigma^{-1}) R(\hat{A}) \right\}^{-1} R(\hat{A})' (I_{NQ} \otimes \Sigma^{-1}) \right] (\Gamma \otimes \Sigma) \left[\left\{ R(\hat{A})' (\Gamma \otimes \Sigma^{-1}) R(\hat{A}) \right\}^{-1} R(\hat{A})' (I_{NQ} \otimes \Sigma^{-1}) \right]' \\ &= \left\{ R(\hat{A})' (\Gamma \otimes \Sigma^{-1}) R(\hat{A}) \right\}^{-1} R(\hat{A})' (I_{NQ} \otimes \Sigma^{-1}) (\Gamma \otimes \Sigma) (I_{NQ} \otimes \Sigma^{-1}) R(\hat{A}) \left\{ R(\hat{A})' (\Gamma \otimes \Sigma^{-1}) R(\hat{A}) \right\}^{-1} \\ &= \left\{ R(\hat{A})' (\Gamma \otimes \Sigma^{-1}) R(\hat{A}) \right\}^{-1} \left\{ R(\hat{A})' (\Gamma \otimes \Sigma^{-1}) R(\hat{A}) \right\} \left\{ R(\hat{A})' (\Gamma \otimes \Sigma^{-1}) R(\hat{A}) \right\}^{-1} \\ &= \left\{ R(\hat{A})' (\Gamma \otimes \Sigma^{-1}) R(\hat{A}) \right\}^{-1}. \end{aligned}$$

□

A.4 Proof of Proposition 3.3

Proof. By Proposition C.15(1) and Proposition 5.1 of Lütkepohl (2005),

$$\text{var} \left\{ \sqrt{T} \left(\hat{\beta}(A) - \beta \right) \right\} = R(A) \left[R(A)' \left\{ \Gamma \otimes \Sigma^{-1} \right\} R(A) \right]^{-1} R(A)'$$

By Proposition C.15(1) of Lütkepohl (2005) and Proposition 3.2 of this paper,

$$\text{var} \left(\sqrt{T} \left(\hat{\beta}(\hat{A}) - \beta \right) \right) = R(\hat{A}) \left\{ R(\hat{A})' (\Gamma \otimes \Sigma^{-1}) R(\hat{A}) \right\}^{-1} R(\hat{A})'$$

Since the covariance matrix $\Gamma \otimes \Sigma^{-1}$ is positive semi-definite, $\{R(A)'(\Gamma \otimes \Sigma^{-1})R(A)\}^{-1}$ and $\{R(\hat{A})'(\Gamma \otimes \Sigma^{-1})R(\hat{A})\}^{-1}$ are positive semi-definite matrices of rank M and \hat{M} , respectively. Therefore, $R(A)\{R(A)'(\Gamma \otimes \Sigma^{-1})R(A)\}^{-1}R(A)'$ and $R(\hat{A})\{R(\hat{A})'(\Gamma \otimes \Sigma^{-1})R(\hat{A})\}^{-1}R(\hat{A})'$ are also positive semi-definite. Given this, and the assumption that $\text{colsp}\{R(A)\} \subseteq \text{colsp}\{R(\hat{A})\}$, we have that

$$\text{colsp} \left[R(A) \left\{ R(A)' (\Gamma \otimes \Sigma^{-1}) R(A) \right\}^{-1} R(A)' \right] \subseteq \text{colsp} \left[R(\hat{A}) \left\{ R(\hat{A})' (\Gamma \otimes \Sigma^{-1}) R(\hat{A}) \right\}^{-1} R(\hat{A})' \right].$$

Thus

$$P := R(\hat{A}) \left\{ R(\hat{A})' (\Gamma \otimes \Sigma^{-1}) R(\hat{A}) \right\}^{-1} R(\hat{A})' - R(A) \left\{ R(A)' (\Gamma \otimes \Sigma^{-1}) R(A) \right\}^{-1} R(A)'$$

has

$$\text{rk} \left[R(\hat{A}) \left\{ R(\hat{A})' (\Gamma \otimes \Sigma^{-1}) R(\hat{A}) \right\}^{-1} R(\hat{A})' \right] - \text{rk} \left[R(A) \left\{ R(A)' (\Gamma \otimes \Sigma^{-1}) R(A) \right\}^{-1} R(A)' \right]$$

nonzero eigenvalues with all other eigenvalues being 0. Hence, P is positive semi-definite and

$$\text{var} \left[\sqrt{T} \left\{ \hat{\beta}(\hat{A}) - \beta \right\} \right] - \text{var} \left[\sqrt{T} \left\{ \hat{\beta}(A) - \beta \right\} \right] \succeq 0. \quad \square$$

A.5 Derivation of the Inverse Marčenko-Pastur Distribution

Suppose $X \sim f_{\text{MP}}(\eta, \sigma^2)$ where

$$f_{\text{MP}}(x; \eta, \sigma^2) = \begin{cases} \frac{1}{2\pi\sigma^2\eta} \sqrt{(x - x_-)(x_+ - x)} & \text{if } x_- \leq x \leq x_+, \\ 0 & \text{otherwise,} \end{cases}$$

is the Marčenko-Pastur distribution with $N/T \rightarrow \eta \in (0, 1)$ as $N, T \rightarrow \infty$, σ^2 being the variance, and

$$x_{\pm} = \sigma^2(1 \pm \sqrt{\eta})^2$$

being the upper and lower bounds of the support of the distribution.

Let $Y = 1/X$. Then the distribution, f_{IMP} , of Y , called the inverse Marčenko-Pastur distribution, has finite support over which its density is

$$\begin{aligned} f_{\text{IMP}}(y; \eta, \sigma^2) &= f_{\text{MP}}(y^{-1}; \eta, \sigma^2) \frac{1}{y^2} = \frac{1}{2\pi\sigma^2\eta y^{-1}} \sqrt{(y^{-1} - x_-)(y^{-1} - x_+)} \frac{1}{y^2} \\ &= \frac{1}{2\pi\sigma^2\eta y^2} \sqrt{[1 - y\sigma^2(1 - \sqrt{\eta})^2][y\sigma^2(1 + \sqrt{\eta}(2-1))]} \\ &= \frac{1}{2\pi\sigma^2\eta y^2} \sqrt{\sigma^4(1 - y)^2 \left(\frac{1}{\sigma^2} \left[\frac{1 + \sqrt{\eta}}{1 - \eta} \right]^2 - y \right) \left(y - \frac{1}{\sigma^2} \left[\frac{1 - \sqrt{\eta}}{1 - \eta} \right]^2 \right)} \\ &= \frac{1 - \eta}{2\pi\eta y^2} \sqrt{(y_+ - y)(y - y_-)}, \end{aligned}$$

where

$$y_{\pm} = \frac{1}{\sigma^2} \left(\frac{1 \pm \sqrt{\eta}}{1 - \eta} \right)^2.$$

Therefore, the distribution of Y is

$$f_{\text{IMP}}(y; \eta, \sigma^2) = \begin{cases} \frac{1 - \eta}{2\pi\eta y^2} \sqrt{(y_+ - y)(y - y_-)} & \text{if } y_- \leq y \leq y_+, \\ 0 & \text{otherwise.} \end{cases}$$

B Applications

B.1 Statistics used in the application to financial returns prediction

Here, we define statistics used in Table 1. Letting $\text{PnL}_t^- := \{\text{PnL}_t : \text{PnL}_t < 0\}$ and $\text{PnL}^- := \{\text{PnL}_t^-\}_{t=1, \dots, T}$, we define the Sortino ratio (Sortino and Price, 1994) as

$$\text{SortR} = \frac{\text{mean}(\text{PnL})}{\text{stdev}(\text{PnL}^-)} \times \sqrt{252}.$$

The maximum drawdown is defined as

$$\text{MaxDrawdown} = \max_{t,s} \left\{ \frac{\text{CPnL}_t - \text{CPnL}_s}{\text{CPnL}_t} : t < s \right\},$$

where $\text{CPnL}_t = \sum_{r=1}^t \text{PnL}_r$. The hit ratio is the mean daily percentage of correct predictions, whereas the long ratio is the mean daily percentage of long predicted positions. The mean absolute error (MAE) and the root mean

squared error (MSE) are defined as

$$\text{MAE} = \frac{1}{TN} \sum_{t=1}^T \sum_{i=1}^N \left| \hat{s}_i^{(t)} - s_i^{(t)} \right|, \quad \text{RMSE} = \sqrt{\frac{1}{TN} \sum_{t=1}^T \sum_{i=1}^N \left(\hat{s}_i^{(t)} - s_i^{(t)} \right)^2}.$$

B.2 Estimating the scale parameter of the Marčenko-Pastur distribution

The scale parameter of the Marčenko-Pastur distribution is chosen as the value of σ^2 that minimises the Kolmogorov-Smirnov statistic:

$$\sigma_*^2 = \arg \min_{\sigma^2} \sup_x |F_{\text{MP}}(x; \eta, \sigma^2) - F_N(x)|, \quad (17)$$

where $F_{\text{MP}}(x; \eta, \sigma^2)$ is the Marčenko-Pastur cumulative distribution and $F_N(x) = k/N$, where k is the number of observations less than or equal to x , is the observed cumulative step-function of the sample eigenvalues of the covariance matrix. The Marčenko-Pastur cumulative distribution is obtained through numerical integration of $f_{\text{MP}}(x; \eta, \sigma^2)$. The minimisation is done using the Broyden-Fletcher-Goldfarb-Shanno algorithm (Fletcher, 2000).

One can also consider embedding the correlation matrix instead of the covariance matrix. In this case, σ^2 is set equal to 1. As an example, Figure 9(a) shows a histogram of the eigenvalues of the covariance matrix used in the FRED-MD application in Section 5.2 after the rows and columns of the design matrix were randomly permuted. The best fit Marčenko-Pastur distribution obtained using Equation (17) is also plotted in Figure 9(a) and fits the histogram well. Figure 9(b) shows a histogram of the eigenvalues of the correlation matrix corresponding to the FRED-MD application in Section 5.2 after the rows and columns of the design matrix were randomly permuted. The Marčenko-Pastur distribution with $\sigma^2 = 1$ is also plotted in Figure 9(b) and fits the histogram well.

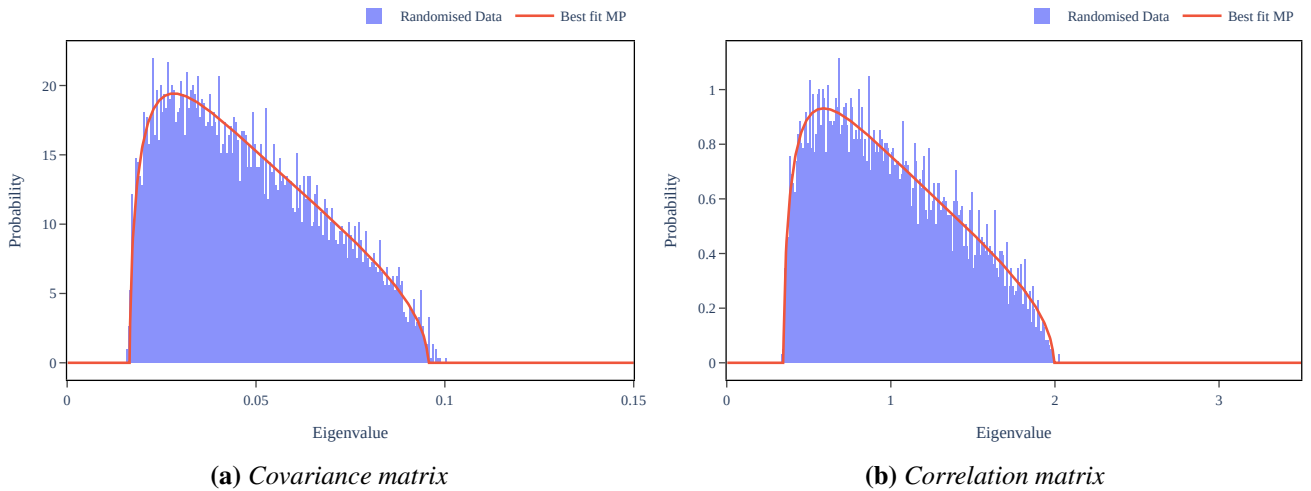


Figure 9: (a) Best fit Marčenko-Pastur distribution alongside the eigenvalues of the covariance matrix used in the FRED-MD application after the rows and columns of the design matrix were randomly permuted. (b) The Marčenko-Pastur distribution with $\sigma^2 = 1$ alongside the eigenvalues of the correlation matrix used in the FRED-MD application after the rows and columns of the design matrix were randomly permuted.